Dr. Matthew Hecht
Handling Topic Editor
Ocean Science

Dear Editor,

Please find attached a new version of the manuscript with number **os-2019-27**, "Seasonal and regional variations of sinking in the subpolar North Atlantic from a high resolution model" which has been modified according to the suggestions and criticisms of two Referees (RC1 and RC2). We also attach a detailed reply letter to the Referees with a list of changes included in the new version of the manuscript, and a version with tracked changes. For completeness, we have included the answer to a short comment (SC1) from Dr. Damien Desbruyères.

We thank both Reviewers to their comments, which have helped us to improve the manuscript and to clarify some fuzzy points. We also thank their appreciation of our work and their generally positive comments. We note that, after our revision, the key conclusions of this work remain unaltered.

The main changes to the manuscript are:

- As suggested by Referee 2, in order to better isolate the overflows in the Iceland-Scotland Ridge, the boundaries of the eastern regions in which we have divided the subpolar North Atlantic have been modified. Numbers in Table 2 and Fig. 6-12 have been updated accordingly. The description of these figures in Sect. 4 has been also updated with the new values for the sinking.
- According to a comment from Referee 2, a new figure (Fig. 9) has been added to the main manuscript describing the vertical transport in the Denmark Strait with an alternative reference system (vertical transport accumulated from the sill).
- Two complementary figures have been added to the supplementary material. The first one, motivated by comments from Referee 2, helps to clarify the up/down bathymetric forced movement of waters in the Irminger Sea (Fig. S9). The other, inspired by the short comment by Dr. Desbruyères, shows more clearly the strong vertical velocities at the edge of the large eddies that develop from the North Atlantic Current in the interior of Newfoundland, nearby the Flemish Cap (Fig.

S4).

- As suggested by Referee 1, Fig. 8 has been moved to the supplementary material (now Fig. S8).
- The origin of the calculation of the accumulated sinking has been shifted from the coastline to depth contour of 50 m. This clarifies the figures, while the conclusions on the existence of different sinking regimes remains unchanged. Fig. 4-5-8 have been updated accordingly.

Other minor modifications are clearly stated in the attached Reply.

We expect that, with the changes and clarifications we have made, our paper will be found suitable for publication in Ocean Science.

Yours sincerely,
Dr. Juan-Manuel Sayol, on behalf of all authors

Referee 1 (RC1):

The present manuscript provides a useful synthesis of a number of recent studies using idealized models and observations of the vertical mass transport in buoyancy driven systems. While it does not present any fundamentally new ideas, it is a useful bridge between the idealized studies and the complexity of the actual North Atlantic system. It is well written and illustrated and I believe it could be published with few if any revisions. I make a few suggestions below that may help clarify a few points but will leave it to the editor to determine if they are ultimately necessary.

■ **Reply 0.** We thank the Referee for his/her comments and time employed in carefully reviewing our work. A point-by-point reply to all questions/concerns/suggestions can be found below.

Major points

1. My first suggestion relates to the choice of origin for the offshore directed coordinate used in the analysis shown in Figs 4, 9, and 11, and the definitions of the Regimes I-III. I suggest that a better choice for the origin would be the shelf break rather than the coast as the broad shelves (e.g. in the Rockall area) play no role in the dynamics under discussion.

■ **Reply 1.** Thank you for this comment, which is also raised by Referee 2 comment 3. The choice of the coast as the origin to accumulate vertical transport has allowed us to uncover sinking regimes (**I-III**), which we believe are useful to reveal qualitatively at which regions the boundary sinking tends to dominate and at which not. However, we agree that the distance to the coast is not very suitable for some regions, such as the overflow areas or Newfoundland. In order to remove part of the undesired shallower shelf from the plots at which no boundary sinking is produced -at the depth of largest sinking-, we have shifted the origin from the coastline to the bathymetric contour of 50 m (C_{50}). So now vertical transport accumulates starting at the closest grid point to a bottom depth of 50 m, and later accumulates other grid points located farther according to their distance to C_{50}. The clearest positive effect is seen in the Labrador Sea, where now sinking starts at 10-20 km from C_{50} in turn of the former 50 km (see Fig. R1 below and Fig. 8 in the new version of the manuscript—note that the eastern regions have been redefined in order to better isolate the Iceland-Scotland overflows as requested by Referee 2, see Fig. R2 or Fig. 6 in the manuscript). Note that according to this new origin, we have redefined the position of the boundaries of sinking regimes, now at 90 and 250 km rather than 110 km and 290 km (Fig. 4 in the manuscript). However, qualitatively results remain very similar, especially for the case of the overflows. For this reason and to give another view (also requested in the major point 1 from Referee 2) an extra Figure (Fig. 9 in the new version of the manuscript) has been added, at which sinking in the Denmark Strait is accumulated according to the distance from the sill that separates the upward and downward movement of water masses.

2. A second, and somewhat related point, concerns discriminating between regions

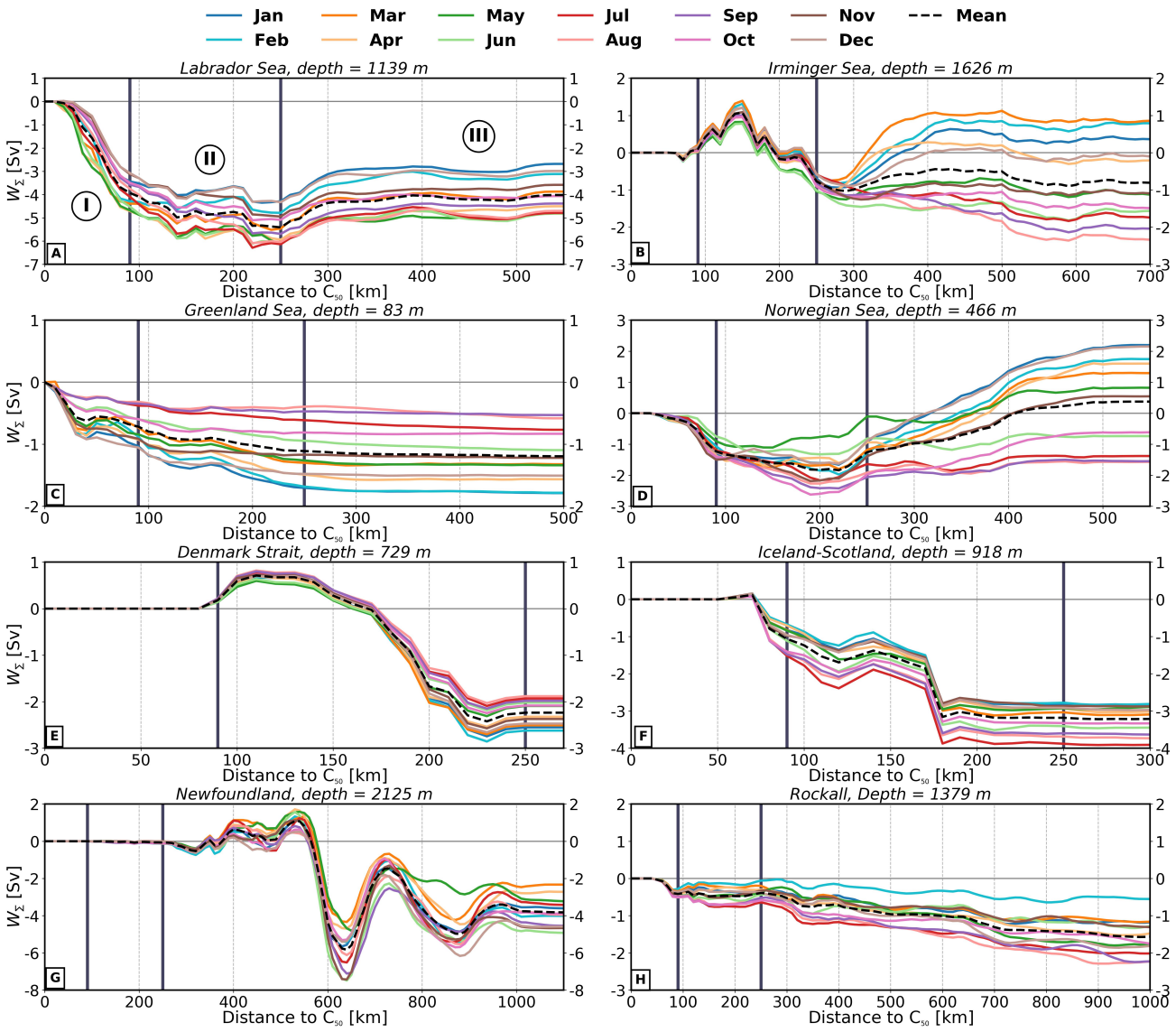

Figure R1: Accumulated net vertical transport (W_Σ) with respect to the distance to the closest bathymetric contour of 50 m (C_{50}). Distances are shown in Fig. 4 (inset map) of the manuscript. Annual (dashed black line) and monthly mean (colored lines) curves are depicted for the regions defined in Fig. 6. The accumulated W_Σ has been calculated at the depth of minimum time-mean W_Σ ($z_{\min}$), which differs for each region (see Table 2 and plot title). The bounds separating the sinking regimes (**I-II-III**) proposed in Fig. 4 of the manuscript (90 km, 250 km) are indicated with thicker solid vertical lines. Note the differences in the horizontal and vertical scales in the plots.

by the slope of the topography. At a number of points in the text (e.g the paragraph following Fig 7), the importance of "steep topography in localizing vertical velocity is discussed. However, no direct quantitative relationship between topographic slope and vertical motion is provided.

■ **Reply 2.** Thank you for this comment, it is an opportunity to clarify it. Steep topography is one of the ingredients that contribute to boundary sinking together with the progressive densification of the boundary current in alongshore direction, a crosshore gradient of density between the interior and the shelf and the existence of eddies. However, a steep topography by itself is not enough to induce boundary sinking since densification of the boundary current is necessary (Spall, 2010; Brüggemann et al., 2017; Brüggemann and Katsman, 2019). One way to isolate the relevance of topography in the boundary sinking is shown in Fig. R3, in which for the whole basin and for each region the depth of largest sinking is plotted against the bottom depth of the corresponding grid point. Overall, it shows that the strongest sinking tends to occur rather close to the bottom, highlighting the relevance of topography. A remarkable exception is Newfoundland, where there is a cloud of points on the right side rather misaligned, likely reflecting the contribution from interior eddies. We have not added Fig. R3 to the manuscript nor in the supplementary material since a similar information can be deduced from Fig. 2B, in which the depth of strongest sinking is very close to the bathymetric contours. Also the new Fig. S9 provides information in the same direction in the Labrador and Irminger Seas. We have reviewed carefully all our expressions in the manuscript that can lead to any misinterpretation regarding the role of steep topography. For instance in the conclusions (Page 28, Ln 16-19):

> *"The near-boundary sinking in regimes **I** and **II** is thought to be governed by the ageostrophic dynamics discussed by e.g. Spall (2010) and Straneo (2006), and its amount depends on the interplay of several factors: the existence of a boundary current, a steep slope, the presence of eddies, and on the along-shore and cross-shore density gradients (sloping isopycnals)."*

Minor points

1. Pg. 6, line 24 : Thea AMOC.

■ **Reply 3.** Corrected.

2. Pg 6, line 31: A clarification that the maximum is taken over monthly means, rather than instantaneous values would be helpful here.

■ **Reply 4.** Thanks. Now it reads (Page 7. Ln 2):

"... obtained from the monthly mean fields"

---

3. Pg 9, line 4: I am looking for a box or some other indication of the region in Fig 2. I assume you mean defined _by_ the domain shown in Fig 2?

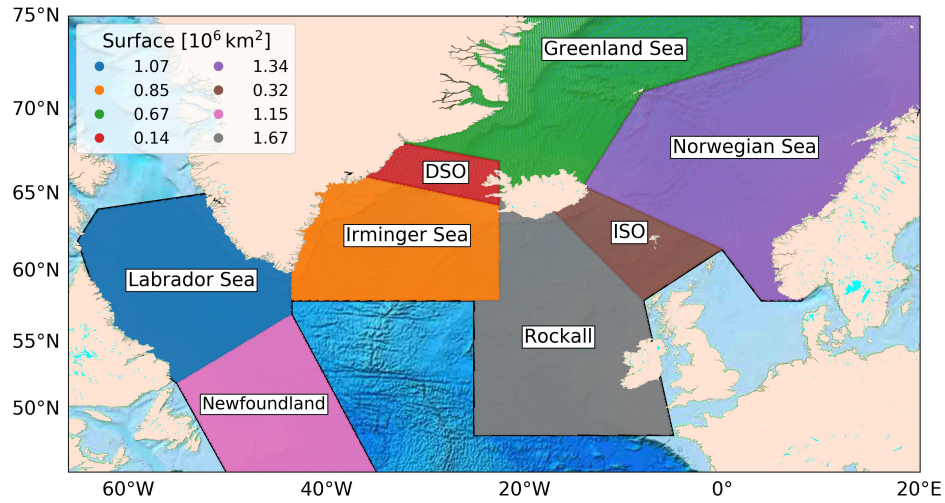

Figure R2: Map of the North Atlantic [66 W − 20 E, 45 N − 75 N] divided into eight regions. DSO and ISO refer to Denmark Strait and Iceland-Scotland Ridge overflow regions respectively. The surface area of each region is shown in the legend in $10^6 \cdot \mathrm{km}^2$.

■ **Reply 5.** Sorry for the lack of clarity. As suggested, it has now been explicitly stated in Page 8. Ln 10.:

"Second, we sum W over the horizontal domain shown in Fig. 2."

---

4. Pg 15, Fig 8: I found little additional information in this Figure beyond that shown in Fig. 7 and Table 2. Could be dropped without loss of support for the text.

■ **Reply 6.** We agree that is not a key figure to understand the main points of this work. However, it nicely shows the seasonal cycle differences among regions, being referred few times in the manuscript. Accordingly this figure has been moved to the supplementary material and now is referred in Sect. 4 as Fig. S8.

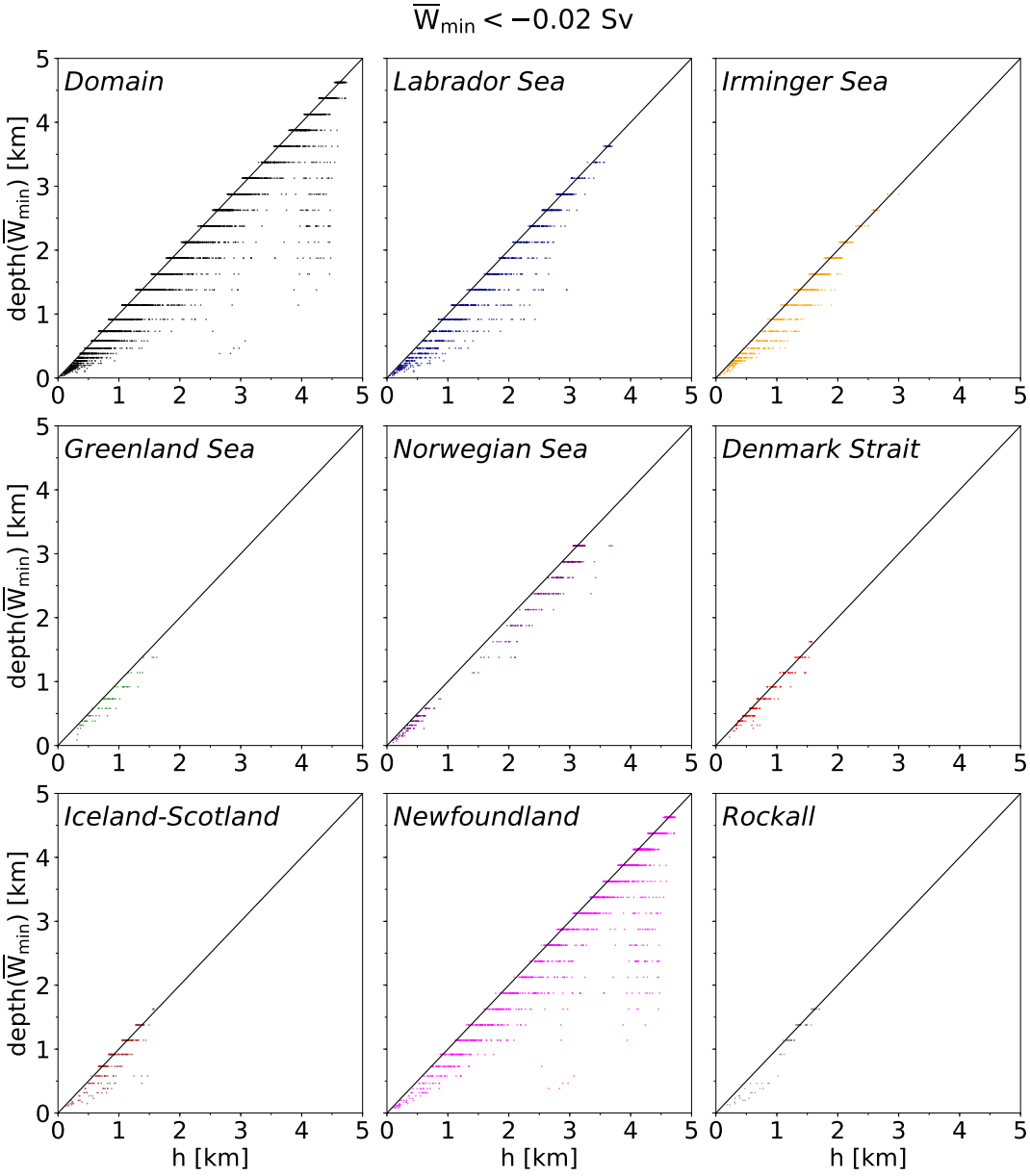

Figure R3: Scatter plots showing the bottom depth (h) and the depth of the mean minimum vertical transport ($\overline{W}_{min}$) for the whole domain (the complete area of Fig. R2) and for each of the regions shown in Fig. R2. Only those grid points with $\overline{W} < 0.02$ Sv are shown. The black line indicates those points where the depth of largest sinking matches the bottom depth.

Referee 2 (RC2):

This manuscript analyzes the vertical velocity in the Atlantic north of 45°N, using 15years of a high resolution simulation forced by a repeating seasonal cycle. As shown in previous more idealized studies, there is net sinking in regions near the ocean boundary, which is highly correlated with the overturning streamfunction at 45N. The unique and original contribution of this manuscript is the examination of the spatial variability of the sinking. While the Labrador Sea is shown to provide a large fraction of the near-boundary downwelling, the Irminger sea has a more complicated signal, and the Newfoundland basin has a vertical motion largely driven by eddies in the interior. The temporal variability of the downwelling signals in these different regions is also different- the Labrador sea has a seasonal signal similar to that of the basin-wide overturning, while the Newfoundland basin has non-seasonal temporal variability driven by eddies. Overflow regions are also shown to behave differently. This paper therefore provides an insight into where and how the downwelling necessary for the AMOC occurs. I therefore support publication. I do however have a few concerns and suggestions for the authors, requiring revision before acceptance.

■ **Reply 0.** We thank the Referee for his/her comments and time employed in carefully reviewing our work. A point-by-point reply to all questions/concerns/suggestions can be found below.

Major points:

1. The overflows: The authors indicate that while the overflow regions do contain significant and important downwelling (together producing as much downwelling as the Labrador sea), the overflow regions do not show the same downwelling mechanism controlled by the lateral boundaries as, for example the Labrador Sea. The authors briefly mention that a key distinction is that the downwelling in the overflow regions is more controlled by bathymetry. I would like to see more attempt to examine the mechanisms in the overflows. Rather than show downwelling aggregated by distance from the nearest land, what would be a better aggregation in the overflow regions - perhaps distance downstream from the sill? I also wonder if the boxes shown for the overflow regions are the best choices, since the downwelling dynamics downstream of the sills could be quite different from upstream. What is the rationale for the ISO box which ex-tends far upstream into the GIN sea? If the DSO box extended further into the Irminger sea (e.g. as far as the region of traceable descent of the dense water downstream of the sill) perhaps the signal from the smaller remaining Irminger box would be less "contaminated"? In summary, I encourage more specific investigation of the overflow regions, using aggregation more suitable to the dynamics in these regions.

■ **Reply 1.** We thank the reviewer for this comment. We agree that the surface of the region

chosen to represent the Iceland-Scotland ridge (ISO) was too big, occupying part of the GIS seas. We have redefined all eastern Atlantic regions: Norwegian Sea, Greenland Sea, Iceland-Scotland Ridge and Rockall. A major consequence is the reduction of the sinking over the Iceland-Scotland Ridge region (ISO), where now only those areas corresponding to the two sills and surroundings have been included (see Fig. R2 of this reply or Fig. 6 in the revised version of the manuscript). Accordingly, Figures 6, 7, 8, 10, 11, 12, S8, S10, S11 and Table 2 have also been modified in the revised version of the manuscript. In terms of sinking, the main changes in the regions of the eastern subpolar Atlantic are (see Fig. 7 and Table 2 of the manuscript for a more detailed description of numbers):

- On average, the Norwegian Sea yields weak upwelling (0.37 Sv) at the depth of largest sinking, although with an increased variability reflected in rather intense net sinking (<-1 Sv) during summer months.

- The Iceland-Scotland region now presents the largest mean sinking at a shallower layer (at 918 m). This sinking is around 0.5 Sv larger than in the former version of the manuscript. The standard deviation is smaller, approaching a value closer to that in the Denmark Strait region.

- The Greenland Sea now reaches the largest sinking in the first 100 m, and it displays a larger seasonal variability. However, sinking remains strong down to a depth of 1500 m, with smaller seasonal variability below 500 m.

- The magnitude of sinking has increased by 0.5 Sv in Rockall. The reason is that the new region contains some sinking near southern Iceland now, while its variability remains rather similar.

Numbers have been updated throughout the manuscript based on these new analysis. Also note that Fig. 8 in former version of the manuscript has been moved to the Supplementary Material (now labelled Fig. S8).

With respect to the request from Referee 2 for a more careful assessment of the overflow dynamics, we have added a new Figure in the manuscript (Fig. R4 below, and Fig. 9 in the new version of the manuscript) that evaluates in more detail the overflows in the Denmark Strait. Thus, upward and downward transports have been computed by considering the distance from the sill (see triangle in Fig. R4A) in the upper and lower DSO regions ($DSO\uparrow$ and $DSO\downarrow$ respectively). These results demonstrate that, on average, water masses upwell as they move southward approaching the sill and sink once they move away from the sill (Fig. R4D). It helps to clarify the upward and downward vertical transport shown in Figure 8E. This figure also shows that results are robust for the defined Denmark Strait region as the grid points that contribute most to sinking are within the first 150 km closest to the sill (Fig. R4D), with little change in the amount of sinking in the subsequent 100 km. Regarding the Iceland-Scotland region, we note that the two sills are still present in Fig. R1F (Fig. 8F in the new version), one at around 80 km from the Faroe Islands (closer to Scotland) and another one at 180 km from the Faroe Islands (closer

to Iceland). We note that some modifications on the origin of accumulated have been applied following suggestions of this Referee (as well as from major point 1 of Referee 1), which are further explained below in the major point 3. To conclude, the discussion of Fig. 9 has been included in Sect. 4.2 (Page 19, Ln 17-26) as follows:

> *"The positive and negative accumulated W_Σ in the Denmark Strait over the first 250 km off C_{50} (Fig. 8E) reflect waters moving southward from the Nordic Seas that first flow up and then down over the sill. This is illustrated by the deepening of the isopycnal in Fig. S6C after crossing the Denmark Strait and demonstrated in Fig. 9, in which the Denmark Strait region has been divided in two parts of similar size on either side of the sill (green triangle in Fig. 9A): one that mainly contains the upward movement of waters as they approach the sill (DSO ↑) and another that contains the downward movement of waters after crossing the sill (DSO ↓). As a result, this up/down transport is clearly reflected in Fig. 9B-C, with the strongest upwelling (+1 Sv) located at a depth of 579 m, and the strongest sinking (−3 Sv) is found at 729 m. The difference between DSO ↑ and DSO ↓ accounts for the near 2 Sv of net sinking found in this region. Furthermore, the accumulated vertical transport with respect to the distance to the sill at the respective depths of strongest upwelling and sinking show that the most important contributions occur within the first 150 km off the sill."*

---

2. The overturning circulation: The overturning circulation shown in figure 1A has several features which may not be realistic - e.g. the large decrease in stream function north of 35N, the very shallow depth, particularly north of 45N. See Dunne et al, 2012 J.Climate, figure 4 for examples of overturning which extend further north and deeper. What connection might there be between the diagnosed pattern of overturning, and the dominant horizontal and vertical locations of downwelling seen in this simulation?

■ **Reply 2.** Despite it is true that the AMOC is not as realistic as it could be, this simulation has some reasonable key features that are further discussed in Section 2 of the manuscript: such as the magnitude of transport in the subpolar Atlantic, the depth of strongest AMOC, its range of variability and the phase of its seasonality. However, in our view the most important point here is that in most simulations and in the observations (RAPID and OSNAP arrays) there is a decrease in the transport of the AMOC between mid-latitudes (30-40°N) and after 45-50°N (also in Dunne et al. (2012), Fig. 8B-C therein). This decrease, by mass conservation, has to be reflected in the amount of sinking in the subpolar region and, although the magnitude of sinking may change between simulations, its regional assessment provides important insights on their distribution and on the physical processes driving it. To state this more clearly, the beginning of Section 3 (Page 6, Ln 25-28) has been modified as follows:

> *"The structure of the AMOC streamfunction (Fig. 1A) indicates that there is a decrease in the amount of transport between the North Atlantic mid-latitudes and the subpolar region that, by mass conservation, must be reflected in the magnitude of the vertical transport. However, such figures only provide a two-dimensional view of the overturning circulation*

in the subpolar North Atlantic. In this study we analyze the complex full structure of the circulation by characterizing spatial and seasonal variations in the sinking."

Regarding the Referee's last question on the connection between sinking and the AMOC that we further discuss in Section 5 of the manuscript; with the present approach we cannot establish a clear connection between the AMOC and the sinking in the sense that we cannot predict how a regional change in sinking will affect the AMOC. For this reason we propose that a Lagrangian assessment can be more suitable to bring more light on this relationship, since it can help to understand pathways of water masses and time scales involved in the variability of boundary sinking and how they propagate to other regions. We are working on this approach at this moment and we expect to show our results in the coming months.

3. Choice of aggregation by distance from the coast: For the overflows in particular, but also for some other regions (e.g. wide shelves compared to narrow shelves), I wonder if there might be a better method of aggregating the downwelling than by distance from the coast. For example, would bathymetric depth be more physically meaningful than distance from the coast? Figure 4 inset shows that distance from the coast gives undue influence to Jan Mayen island in the Greenland sea, for example. If the downwelling occurs next to the topography, we might expect to see a close relationship between the depth of maximum downwelling and the bathymetric depth, which is hidden when aggregating by distance from land.

■ **Reply 3.** Also following a similar question from Referee 1 (major point 1), we have reduced the undesired effect of the shelf in Fig. 4 and Fig. 8 of the manuscript by accumulating sinking with respect to the closest contour of 50 meters of depth (C_{50}) in turn of the coastline (see Fig. 4 and Fig. 8 in the revised version of the manuscript or Fig. R1 here). This modification, together with the redefinition of the eastern regions (specially the ISO region) and the inclusion of Fig. R4 (Fig. 9 in the new version of the manuscript) helps to clarify the overflow dynamics. Following the Referee's suggestion we have also tried to accumulate sinking using other approaches, e.g. with respect to the bottom depth. Although consistent with the magnitude of sinking, these other approaches are significantly harder to explain (and sinking regimes more difficult to visualize) than the simpler horizontal vision shown in Fig. R1.

The connection between sinking and topography is highlighted in Fig. R3, where the bottom depth is plotted against the depth of largest sinking for the whole domain and for individual regions (defined in Fig. R2). We note that only those grid points with intense sinking ($W_{min} < -0.02$ Sv are shown. As suggested by the Referee, a close linear relationship is evident between topography and sinking, remarkably in the Labrador, Irminger and Newfoundland Seas. Besides there are some misaligned points on the right side of Newfoundland that we associate with sinking within the interior eddies (see a more detailed response on Newfoundland eddies in the reply to the short comment, SC1). We note that Fig. R3 has not been added to the manuscript nor the supplementary material since a similar information can be deduced from Fig. 2B, in which the depth of the near-boundary strongest sinking is very close to the bathymetric contours. Also the new Fig. S9, discussed below, provides information in the same direction in the Labrador and Irminger Seas.

4. Interpretation of upwelling: I find it hard to interpret the upper ocean/near boundary upwelling seen in the Irminger sea (figure 7B and 9B), and the near boundary upwelling seen in the Denmark Straits (figure 9E). What does this imply physically - how is the circulation closed, where is the upwelled water going? Would a section, showing velocities binned by horizontal and vertical distance, help provide more information?

■ **Reply 4.** The comment on the Denmark Strait has been addressed in major point 1, so we now focus on the Irminger Sea. To this we have selected a section across the Irminger Sea (Fig. R5, see location of section in the inset within panel A), where the shading color indicates the perpendicular component of velocity (v) and we have depicted the tangential velocity and the vertical velocity (u, $1000 \times w$) field by black arrows. Overall this figure shows an offshore component of v (indicated by the dominant blue color, i.e. waters move out of the paper) suggesting that the bathymetry is pushing the water off the slope) as well as a persistent upward and downward vertical movement of waters during the all year that shows little change in intensity (compare A-D panels). The vertical flow seems to be mostly driven by bathymetric features since the transport is more intense near the bottom. Interestingly, these vertical displacements of water may propagate long distances upward (>1000 m) even sometimes reaching almost the surface layers thus suggesting a rather barotropic behaviour of the water column. We note that Fig. R5 has not been included in the manuscript nor in the supplementary material because we have included Fig. S9, which is described in the reply to major point 5 and complements this reply on the Irminger Sea upwelling.

5. Small scale motion of alternating sign: In figure 2A, I have difficulty seeing a clear signal of net downwelling in any region around the northern boundary because of the large amplitude signals of alternating sign. Whereas the mean Labrador sea signal in figure 7 is for near-boundary downwelling, the mean Irminger sea signal is for near-boundary upwelling, yet in figure 2A, the two regions look qualitatively similar, with large amplitude alternating signals. Is it possible to apply a spatial filter to the fields in figure 2A, to show what the vertical motion looks like when averaged over the eddy scales? Its also not clear to me why the Irminger sea alternating signal is suggested to be tied to topography - are there features in the bathymetry on these scales? If so, aggregating by bottom depth might be a way to clarify.

■ **Reply 5.** We agree with the Referee. The resolution of Fig. 2 of the manuscript is not good enough to appreciate all these subtleties. To clarify this point a new figure considering the vertical transport in the Labrador and Irminger Seas has been made (Fig. R6). First, the mean W at a depth of 1139 m is shown in the near-boundary region of Labrador and Irminger Seas with shading color. It allows to see clearer the coherent patterns of up and down vertical transport. Next, over the bathymetric contour depth of 1800 m (see gray contour line in the main panel) we have estimated the mean vertical transport, W at a depth of 1139 m (shading color). Then we have plotted it starting in the Labrador Sea and finishing in the Irminger Sea (see inset in Fig. R6). The separation between both seas according to the regional map shown in Fig. R2 is

also denoted by a dashed vertical dark red line. This plot shows the main differences in sinking patterns between both seas, which are characterized by a more erratic shape in the Labrador Sea and a clearer up and down movement in the Irminger Sea, specially at distances >600 km. It also helps to stress (together with Fig. R5) the key role that bathymetric features play in the Irminger Sea. For completeness this figure has been added in the Supplementary Material as Fig. S9 and is referred in Sect. 4.4 as follows:

> *In contrast to the Labrador Sea, the change in W in the Irminger Sea between the months of minimum and maximum time-mean W_Σ is significantly smaller (Fig. 10B). This finding, together with the permanent depth of largest sinking ($z_{\min}$) and the up and down distribution of sinking found in Fig. 8B, supports the hypothesis that the sinking near the boundary in the Irminger Sea is mostly quasi-stationary and topographically-driven (see a detailed example of this up/down of waters in Fig. S9), which explains the small amount of net sinking found.*

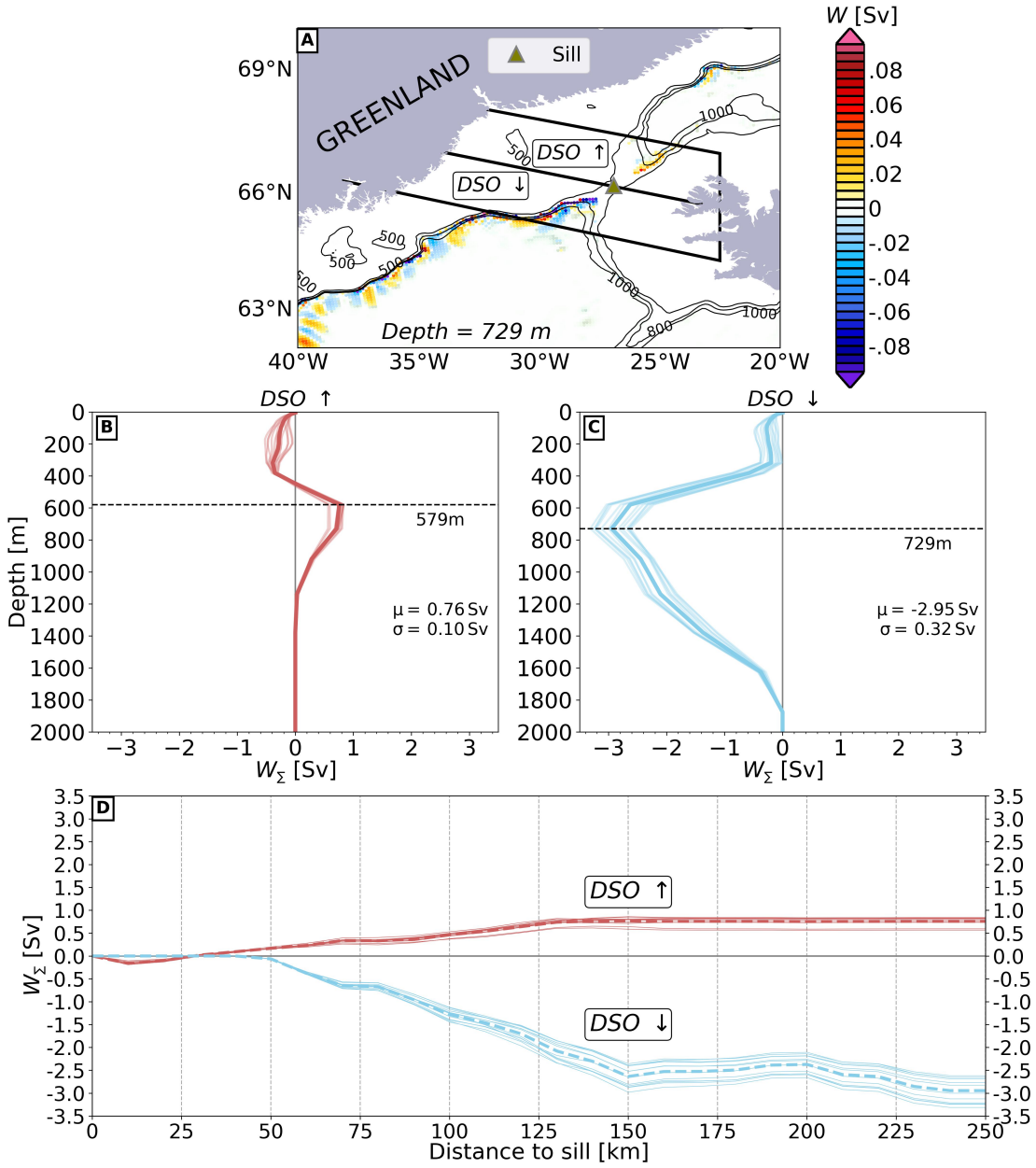

Figure R4: (A) Map of Denmark Strait Overflow region (DSO). The mean vertical transport (W) at 729 m is depicted by shading (color). The triangle illustrates the location of the sill (green triangle) that separates the Denmark Strait in two areas of similar size (DSO ↑ and DSO ↓). Bathymetric contours are indicated by black line. (B-C) Vertical structure of transport (W_Σ) in DSO ↑ and DSO ↓ respectively. (D) Annual (dashed line) and monthly (red solid lines) accumulated vertical transport with respect to the sill in DSO ↑ (red) and in DSO ↓ (light blue). Both have been calculated at the corresponding depths of largest upwelling (579 m) and sinking (729 m) for DSO ↑ and DSO ↓ respectively.

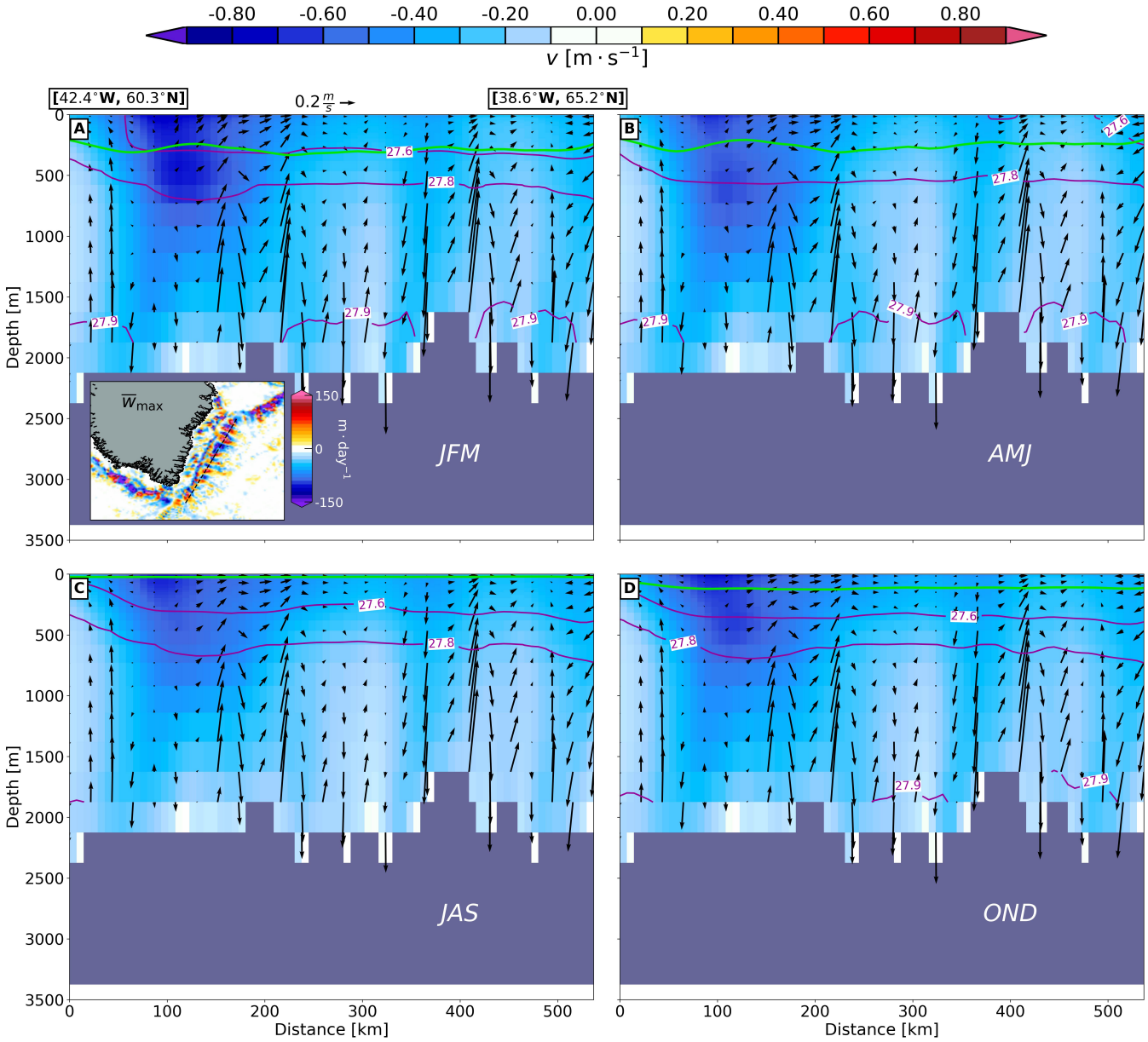

Figure R5: 15-year climatology of the velocity field at a cross-section between the southern tip of Greenland and the southern limit of the study area (see inset in panel A). Each panel represents a seasonal average: (A) JFM (January-February-March); (B) AMJ (April-May-June); (C) JAS (July-August-September); OND (October-November-December). The shading shows the normal velocity component (indicated by v), with units in $\mathrm{m\,s^{-1}}$; black arrows are velocity vectors constructed as $(u,\, 1000 \cdot w)$ where u and w are the tangential and the vertical velocity components respectively. For clarity arrows are shown for selected depths and grid points. The green line depicts the seasonal mean mixed layer depth (in m), while the black contours denote the seasonal potential density anomaly, $\sigma_\rho = \rho - 1000$.

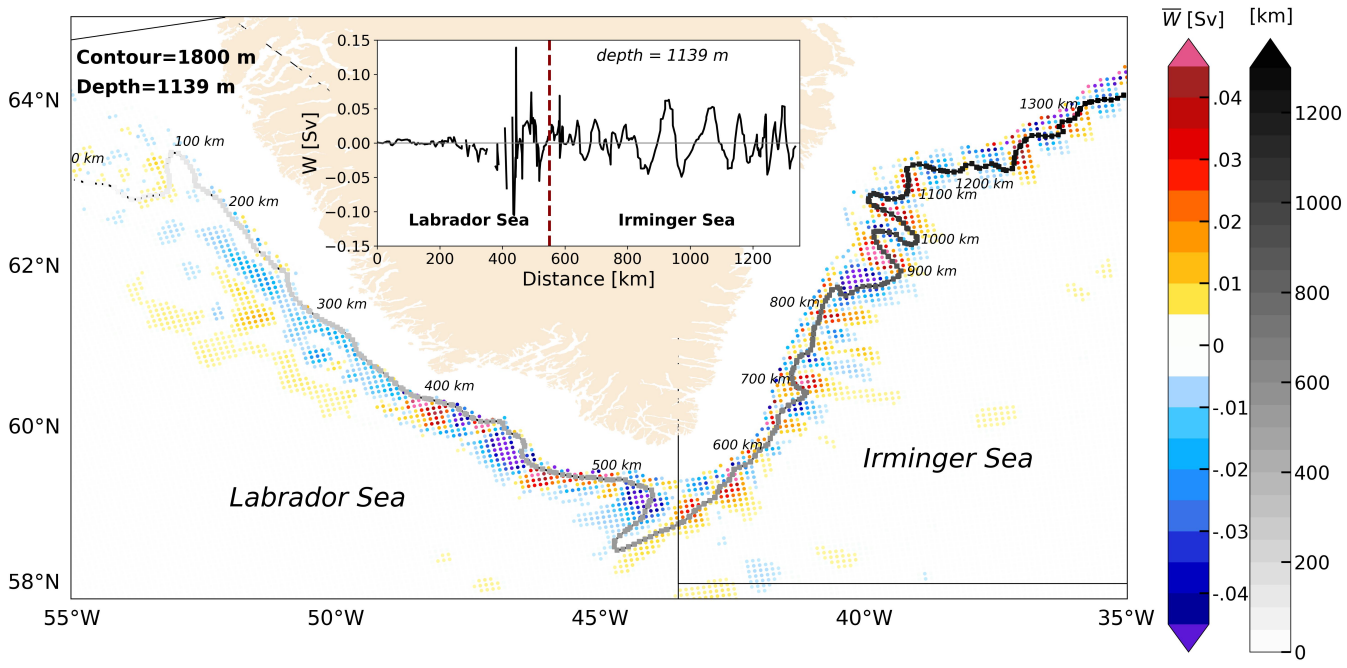

Figure R6: Mean vertical transport (W) at a depth of 1139 m (shading color) in Sv. The grayscale contour indicates the bathymetric contour of 1800 m. Its grade of colors denotes the distance over this contour from southwestern Greenland to southeastern Greenland in km. The inset panel shows W at the those grid points located at the contour of 1800 m at a depth of 1139 m according to the distance defined in the main panel. The vertical dark red dashed line marks the boundary between Labrador and Irminger Seas according to Fig. 6.

Specific comments:

Page 2, Line 3: Insert "few" after "Over the last"

■ **Reply 6.** Done.

Page 2, Line 31: Change "looses" to "loses".

■ **Reply 7.** Thank you. This typo has been corrected.

Page 3, Line 28: Change "and idealized eddy-resolving model" to "an idealized eddy-resolving model".

■ **Reply 8.** Done.

Page 4, line 3-4: "not adding even more complexity" - Im not sure what you mean by this, perhaps not adding the additional complexity of historical variations in surface forcing?

■ **Reply 9.** As suggested we have redone this unclear statement. Now it reads:

To this end, we use an ocean-only eddy-resolving numerical simulation with a nominal resolution of 0.1° *under a repeated climatological annual atmospheric forcing, not adding the additional complexity of historical variations (e.g. at inter-annual or inter-decadal scales) in surface forcing.*

Page 6, line 20-21: Change "Nevertheless it can be inferred a stronger transport in winter than in summer" to "Nevertheless, a stronger transport in winter than in summer can be inferred . . . "

■ **Reply 10.** Done.

Figure 2B: The depth color bar shows increasing depth upward, whereas it is more intuitive to show it downward on the color scale (a minor point, I know)

■ **Reply 11.** The colorbar has been reversed accordingly.

Figure 3: Given this downwelling in Sv, if you divided through by the area at each depth,what would this imply for the magnitude of the vertical velocity in m/s? How does this compare with the magnitudes shown in figure 2A? (Im guessing that the noise shown in figure 2A is much greater than the mean signal).

■ **Reply 12.** For the Labrador Sea case, the surface at the depth of 1139 m is around $7{\cdot}10^6 \mathrm{km}^2$. Then, for a total downwelling of 4 Sv the mean vertical velocity is around 0.5 m/day. In this regard we note that we are using monthly mean fields and therefore the strong velocities found in the boundary respond to some averaged physical processes. Additionally, the up and down pattern of vertical transport shown in Fig. R6 appear to be rather spatially coherent and not isolated spots. Additionally the values of standard deviation in Fig. 2C are rather smaller (around 5 times) than the near boundary vertical velocities shown in Fig. 2A. Therefore we are convinced that the near-boundary sinking is not noise. It has been explicitly stated in Page 7 Lines 8-10 as follows:

"These strong vertical velocities velocities cannot be considered as noise since they show a coherent spatial pattern along the bathymetric contours and their standard deviation is several times smaller (square root of variance shown in Fig. 2C, about 30 m day 1) than their mean value."

---

page 10, line 4-5: If the W value is shown at a depth of 1139 m, what do you do if the grid cell bathymetry is shallower than that value?

■ **Reply 13.** Then it is assumed that there is no value to be added. It has been explicitly stated in the caption of Fig. 4:

*"Cumulative net vertical transport (W_Σ) at a depth of 1139 m (in Sv) as a function of the distance from the bathymetric contour of 50 m depth referred to as C_{50} (inset map in Fig. 4). If the grid cell bathymetry is shallower no value is added. The dashed black line shows the annual mean. Monthly values of the 15-year simulation are shown in light gray, colored lines indicate the monthly climatology. The regimes of sinking are indicated by roman numbers **I-II-III**, and the separation lines between them are also denoted by a brown and a black triangle and by contours in the same color in the inset figure."*

---

p11 discussion of figure 5, and figure 5: To see the context of the currents around 1250km-1000km south of Greenland, it would be helpful to show an inset of the surface currents over the whole North Atlantic. How is this "standing eddy" related to the North Atlantic Current?

■ **Reply 14.** We have added the main surface features around the section in the inset of Fig. 5 of the manuscript. However, due to the small size of the inset for a complete view of the mean North Atlantic circulation we refer to Fig. S1 (top panel) in the Supplementary Material. Also Fig. R7 (labelled Fig. S4 in the supplementary material) provides a good view of the currents near the Flemish Cap.

Regarding the eddies, large eddies are detached from the North Atlantic current as it meanders on their way to the North (see Fig. R7). These eddies move around the Flemish Cap and few of them even propagate northwestward into the central Labrador Sea. Indeed they can stay for months nearby the Flemish Cap region before dissipating. The big red/blue patches of W in Fig. 10 of the manuscript are a good indicator of the vigorous eddy field present in Newfoundland and of their role on the marked upward/downward motion that we find there.

page 26, lines 30-31: Change "limit us to find" to "prevents us from finding".

■ **Reply 15.** Done.

page 27, line 5: Change "isopycnals significantly fluctuate" to "isopycnals fluctuate significantly"

■ **Reply 16.** Done.

Short Comment (SC1) from Damien Desbruyères

I have a question regarding the particular region of Flemish Cap, where you report a relatively important eddy-driven sinking. I wonder how the latter reconciles with the key ingredient for vertical sinking: a positive along-stream density gradient supporting an in-shore geostrophic flow in the upper layer. Through mass conservation this drives downwelling along the slope, as the authors well explained in their introduction. This is not the case of the boundary current encircling Flemish Cap, which is warming as it flows downstream due to exchanges with the warmer North Atlantic Current, so that the sign of the along-stream density gradient would rather suggest upwelling there. Could the authors comment on this?

■ **Reply 1.** First of all thank you for your interest in our work. We think that the term "eddy-driven sinking" (or eddy-induced, a term that we also use) is ambiguous, since it could be used for any of the sinking regimes (**I-II-III**). Surely it has given place to an inaccurate interpretation of our words. The reason in that in the near-boundary sinking (at around 1000 m, closer to the shelf) as well as in the offshore sinking (that sometimes extends below 2000 m and is found farther offshore), eddies play a central role although in a very different dynamical way.

In the following lines we discuss the dynamics around and off the Flemish Cap in order to bring more light on the dynamical processes occurring there according to our model simulation. First, this region is characterized by a strong front, as indicated by the contours of potential density anomalies (black thick contours) in Fig. R7A-B, in which A-B panels correspond to two different depths (FC refers to Flemish Cap). The strength of this front is illustrated by the decrease in about 0.6 $\mathrm{kg \cdot m^{-3}}$ in $\sim$ 200 km when we move off the eastern side of Flemish Cap . However, below 1000 meters the potential density is rather homogeneous around the Flemish Cap, with almost constant values of $28.01 - 28.02\, kg \cdot m^{-3}$ at 2125 m (some insight can be inferred from Fig. S6C in the supplementary material) that change little along the current pathway (see trajectory in Fig. R7C-D). Based on this, a major relevance of other sinking mechanisms different from the near-boundary sinking is expected to explain the strong vertical velocities seen (shading in Fig. R7).

Indeed from Fig. R7C-D we can infer that as the current approaches to the Flemish Cap, it first moves up as it faces shallower bathymetric contours (see the dominant red patch in the northwestern Flemish Cap in Fig. R7C-D), and later moves down as water finds a deeper bathymetry (see the subsequent blue patch). This explains the up/down closer to the Flemish Cap which should be roughly compensated to provide little net transport (as it is indicated by the small sinking in the first 200 km found in Fig. R1G or Fig. 8G in the manuscript).

However, if now we move a bit farther off the Flemish Cap to the interior of Newfoundland, also large blue and red patches appear at the edges of mesoscale eddies (indicated by the enclosed black arrows). In this case, the upward/downward movement of waters is governed by the own eddy dynamics, which is also different from near-boundary sinking. The reason of this sinking at the edges is unclear for us and will require further study, which is not attainable with the monthly fields used here. Some works have mentioned the fast vertical displacement of isopycnals as one plausible cause for strong vertical velocities of mesoscale geostrophic eddies, e.g. Viúdez

and Dritschel (2003). Therefore, if near-boundary sinking exists in this region, it is rather limited and hardly comparable to the one in the Labrador Sea, as suggested by Fig. R1G (Fig. 8G in the manuscript).

We hope that this explanation will clarify more the processes occurring within the Newfoundland region, as well as the processes that can be seen in Fig. 5 of the manuscript. Fig. R7 has been added to the supplementary material as Fig. S4. In the new version of the manuscript we have avoided the expression eddy-driven (eddy-induced) sinking when we refer to the sinking that occurs farther offshore at the edge of large interior eddies (regime **III**). The main changes are indicated below.

- In Sect. 3.1 (Page 8. Ln 1-6):

  "The positive and negative alternations offshore of the Flemish Cap and in the interior of Greenland and Norwegian Seas must have a different cause. In the case of the Flemish Cap, they occur at the edges of eddies (Fig. S4) and the depth of largest sinking is below 2000 m (Fig. 2B, also in the interior of Norwegian and Greenland Seas), which indicates these eddies are deep and possibly have a strong barotropic component. Indeed, the high variance of vertical velocities in the surroundings of the Flemish Cap ($\sigma^2(w)$) is a reflection of the existence of an active eddy field throughout the year (Fig. 2C). Also the subsurface EKE shows this signal (Fig. S5)."

- The last paragraph of Sect. 3 (Page 13, Ln. 19-23) has been rewritten as follows:

  *"Finally, the sinking in regime **III** is related to those processes that develop away from the shelf and far from the core of the boundary current. In this case, strong vertical velocities appear at the edge of interior eddies, which are governed by a different dynamics (Fig. 5). The major role of such quasi-permanent eddies is supported by the marked fluctuations between 300 and 1000 km in Fig. 4, the large interior eddy in Fig. 5 and the vigorous EKE field in the interior of the Newfoundland Basin, near the Flemish Cap (Fig. S4 and Fig. S5)."*

- The last paragraph in Sect. 4 (Page 24, Ln. 4-12) has been rephrased to avoid any ambiguity:

  *"Newfoundland yields the second largest contribution to sinking, which is largely produced within the sinking regime **III**. The strong seasonal variations of W in the Newfoundland region below 2000 m are mostly related to EKE interior pathway changes (see black contours in Fig. 10B) impinged by North Atlantic Current fluctuations and meandering. The fact that strong vertical velocities appear at the edge of large eddies in the interior, thus contributing to upwelling/sinking has been already shown in Fig. 9G, Fig. 10A-B and Fig. S4, where a train of large eddies near the Flemish Cap is visible). Finally, in the Newfoundland region the peak of the boundary current at its corresponding $z_{\min}$ falls in regime **III** (Fig. 11E); although the strongest sinking occurs in the interior and below 2000 m, there is some sinking at shallower depths as indicated by its vertical structure in Fig. 7G (Fig. S4). Similar plots showing the overall weaker spatial patterns of sinking for the remainder of the regions can be found in Fig. S10 and Fig. S11."*

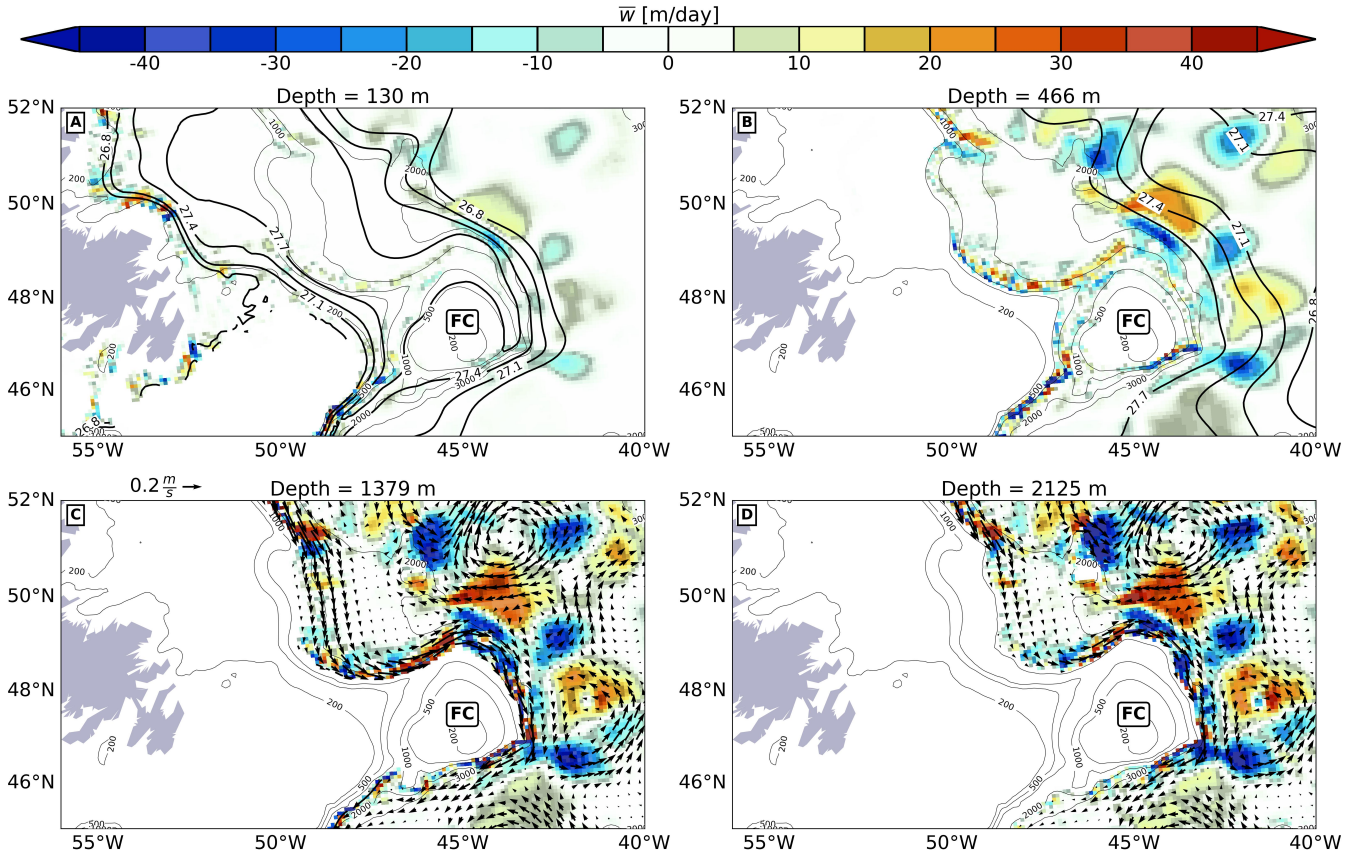

Figure R7: Mean vertical velocity at different depths around the Flemish Cap ($\overline{w}$): (A) depth of 130 m, (B) depth of 466 m, (C) depth of 1379 m, (D) depth of 2125 m. Thin contours represent bathymetry in all panels. Black thick contours in (A-B) represent the potential density anomalies. Black arrows in (C-D) denote the horizontal current fields. For all cases the 15-year mean is shown. FC refer to the Flemish Cap.

References

Brüggemann, N. and Katsman, C. A. (2019). Dynamics of downwelling in an eddying marginal sea: contrasting the Eulerian and the isopycnal perspective. *Submitted to Journal of Physical Oceanography*.

Brüggemann, N., Katsman, C. A., and Dijkstra, H. A. (2017). On the vorticity dynamics of the downwelling branch of the AMOC. *CLIVAR Exchanges Special Issue: CLIVAR Open Science Conference Award Winners*, 71:10–12.

Dunne, J. P., John, J. G., Adcroft, A. J., Griffies, S. M., Hallberg, R. W., Shevliakova, E., Stouffer, R. J., Cooke, W., Dunne, K. A., Harrison, M. J., Krasting, J. P., Malyshev, S. L., Milly, P. C. D., Phillipps, P. J., Sentman, L. T., Samuels, B. L., Spelman, M. J., Winton, M., Wittenberg, A. T., and Zadeh, N. (2012). GFDLs ESM2 Global Coupled ClimateCarbon Earth System Models. Part I: Physical Formulation and Baseline Simulation Characteristics. *Journal of Climate*, 25(19):6646–6665.

Spall, M. A. (2010). Dynamics of Downwelling in an Eddy-Resolving Convective Basin. *Journal of Physical Oceanography*, 40(10):2341–2347.

Straneo, F. (2006). On the Connection between Dense Water Formation, Overturning, and Poleward Heat Transport in a Convective Basin. *Journal of Physical Oceanography*, 36(9):1822–1840.

Viúdez, A. and Dritschel, D. G. (2003). Vertical velocity in mesoscale geophysical flows. *Journal of Fluid Mechanics*, 483:199–223.

Seasonal and regional variations of sinking in the subpolar North Atlantic from a high-resolution ocean model

Juan-Manuel Sayol[1], Henk Dijkstra[2], and Caroline Katsman[1]

[1]Department of Hydraulic Engineering, Delft University of Technology, Delft, The Netherlands

[2]Institute for Marine and Atmospheric research Utrecht, Utrecht University, Utrecht, The Netherlands

Correspondence: Juan-Manuel Sayol (J.M.SayolEspana@tudelft.nl)

Abstract. Previous studies have indicated that most of the net sinking associated with the downward branch of the Atlantic Meridional Overturning Circulation (AMOC) must occur near the subpolar North Atlantic boundaries. In this work we have used monthly mean fields of a high-resolution ocean model (0.1 deg at the equator) to quantify this sinking. To this end we have calculated the Eulerian net vertical transport (W_Σ) from the modelled vertical velocities, its seasonal variability and its spatial distribution under repeated climatological atmospheric forcing conditions. Based on this simulation, we find that for the whole subpolar North Atlantic W_Σ peaks at about -14 Sv at a depth of 1139 m, matching both the mean depth and the magnitude of the meridional transport of the AMOC at 45°N. It displays a seasonal variability of around 10 Sv. Three sinking regimes are identified according to the characteristics of the accumulated W_Σ with respect to the distance to the ~~coast~~shelf: one within the first ~~110~~ 90 km and onto the bathymetric slope at around the peak of the boundary current speed (regime **I**), the second between ~~110 km and 290~~ 90 km and 250 km covering the remainder of the shelf where mesoscale eddies exchange properties (momentum, heat, mass) between the interior and the boundary (regime **II**), and the third sinking regime at larger distances from the ~~coast~~ shelf where W_Σ is mostly driven by the ocean's interior eddies (regime **III**). Regimes **I** and **II** accumulate $\sim 90\%$ of the total sinking and display smaller seasonal changes and spatial variability than regime **III**. We find that such a distinction in regimes is also useful to describe the characteristics of W_Σ in marginal seas located far from the overflow areas, although the regime boundaries can shift a few tens of km inshore or offshore depending on the bathymetric slope and shelf width of each marginal sea. The largest contributions to the sinking come from the Labrador Sea, the Newfoundland region and the overflow regions. The magnitude, the seasonal variability and the depth at which W_Σ peaks vary for each region, thus revealing a complex picture of sinking in the subpolar North Atlantic.

1 Introduction

The Atlantic Meridional Overturning Circulation (AMOC) is a fundamental component of the Earth's climate system (Lozier, 2012; Buckley and Marshall, 2016). Over the last few decades the traditional view of an ocean conveyor with an upper poleward current transporting warm waters to higher latitudes, and a downward branch with intermediate and deeper denser waters that originate in the regions of deep convection and move toward the equator (Broecker, 1987, 1991) has been revised.

First, it became apparent that eddies actively mediate between the upper and lower limbs of the AMOC (Lozier, 2010). As a consequence, the Deep Western Boundary Current (DWBC) presents large spatio-temporal variability, as the flow splits in the North Atlantic (near $50°$ N) in the well-known western current aligned with the boundary (Stommel and Arons, 1959) and other more elusive interior paths (Bower and Hunt, 2000; Bower et al., 2009). Similarly, at the surface, the pathways of the North Atlantic Current that connect the subtropical gyre with the subpolar gyre are still not well established, as evidenced by the trajectories of surface drifters (Brambilla and Talley, 2006) and by estimates of the inter-gyre exchange (Rypina et al., 2011).

Second, the earlier idea that strong open ocean convection -e.g. in the interior of the Labrador, Irminger or Greenland Seas- is accompanied by large-scale sinking of waters, and that this downwelling represents the largest part of the sinking related to the AMOC, has been abandoned. The explanation for this is that once the winter cooling has preconditioned the convection site through a prolonged buoyancy loss, the vertical transport associated with small-scale (~ 1 km) deep convective plumes is mostly compensated by nearby rise of waters, so that little vertical mass transport is expected (Marshall and Schott, 1999; Send and Marshall, 1995). Moreover, these regions of deep convection are highly localized, with length scales of 500 km of less. This implies that the horizontal gradient in planetary vorticity across the convection region is small. In order to balance the vorticity changes associated with substantial sinking in the geostrophic ocean interior, an unrealistically strong northward current would be required (Spall and Pickart, 2001). Instead, previous studies have shown that the Eulerian net sinking (in depth space) associated with the lower branch of the AMOC must occur near the boundaries, where the flow is subject to non-geostrophic dynamics. Thus, at the topographic slopes a richer vorticity balance arises with a dissipation term that compensates the vertical stretching of planetary vorticity induced by the sinking (Spall and Pickart, 2001; Spall, 2004, 2008; Brüggemann et al., 2017). As a result, higher rates of sinking are attainable near the boundaries of marginal seas.

Spall and Pickart (2001) and Pedlosky and Spall (2005) analyzed the sinking along a straight boundary current subject to buoyancy loss. They found that a flow in thermal-wind balance develops, with a density gradient that spirals with depth. Such a spiraling structure induces strong vertical movements, which they found to be proportional to the along-shore density gradient and the mixed layer depth. With a 2-layer approach, Straneo (2006) studied a boundary current surrounding denser interior waters as a representation of the Irminger Current waters flowing around the perimeter of the Labrador Sea. In her model net sinking appears in the boundary layer as the boundary current ~~looses~~ loses buoyancy along the perimeter. She also found that larger along-shore density gradients give rise to more sinking. Consistently Cenedese (2012) came to a similar conclusion from laboratory experiments in a tank. However, the North Atlantic is not the only place where sinking predominantly takes place near the boundaries. As pointed out by the recent work of Waldman et al. (2018), significant sinking occurs in the first 50 km off

the coast in the Mediterranean Sea, though it is much smaller than in the North Atlantic (~ -1 Sv, where $1\,\mathrm{Sv} = 10^6\,\mathrm{m^3\,s^{-1}}$). At this location, sinking is catalyzed by the existence of a western boundary current that densifies along its way around the basin, a strong winter cooling in the interior due to northerly winds, and an active near-shelf eddy field.

More recently, Katsman et al. (2018) estimated the net sinking in the North Atlantic from model simulations at a depth chosen to match the maximum of the overturning streamfunction (at 1060 m), well below the mixed layer depth. They computed the net sinking over the time averaged fields of two hindcasts based on the same ocean model (ORCA) and atmospheric forcing. The two simulations covered the period 1958-2001 and had a different horizontal resolution (0.25° and 1°, —ORCA025 and ORCA1— respectively). Their results showed a significant net sinking along the boundaries, much higher than in the interior. Notably the finer resolution model displayed 8 Sv more net sinking along the perimeter than the lower resolution version (-20 Sv and -12 Sv respectively). However, the contribution of overflow waters to the total budget of net sinking along the selected perimeter was nearly the same in absolute terms, with average amounts of -7.6 Sv and -7.4 Sv for the coarser and the finer resolution simulation respectively. Hence, the large differences in sinking between both simulations are mostly attributed to the boundary region. According to the authors, this difference may be due to the fact that the finer resolution model is eddy permitting. Thus, ageostrophic eddy-driven processes may also play an important role in boundary sinking. For instance, eddy-induced heat fluxes significantly increase the lateral heat exchange between the cooler interior and the warmer boundary, cooling the boundary current on its way and then enhance the along-shore density gradient (Spall, 2011). Also, as pointed out by Spall (2010) eddy vorticity fluxes and dissipation play an important role in balancing the vertical stretching of planetary vorticity induced by sinking in a convective basin.

In order to better understand the contribution of geostrophic and ageostrophic processes to sinking ~~,~~Brüggemann and Katsman (2019) used an idealized model with fine resolution (3 km in the horizontal), which is able to mimic the basic features of the Labrador Sea: a cyclonic boundary current circulating along a semicircular basin, with a small part dominated by a steeper topographic slope (change in depth of 3000 m in few tens of km) resulting in the generation of a vigorous eddy field. Stronger sinking was found onto and near the sharp topographic feature than in any other place in the domain. ~~To quantify the importance of all involved processes in the amount of net sinking the authors decomposed the vorticity balance separating mean from eddy terms; it included the stretching of planetary vorticity, the mean and eddy horizontal advection of vorticity as well as the β and dissipation terms. One important result is that the intense vertical stretching of planetary vorticity associated with the sinking is balanced by the horizontal advection of vorticity and dissipation.~~ Likewise, the recent work of Georgiou et al. (2019) highlights the importance of eddy-driven transport using ~~and~~ an idealized eddy-resolving model of the Labrador basin. Among others, this study demonstrates that the total amount of sinking is sensitive to changes in the eddy pathways. It must be stressed here that the above idealized studies assumed closed basins, while in reality open boundaries exist and exchanges between the North Atlantic and Arctic occur. Overflows also contribute significantly to the net sinking, as shown in Katsman et al. (2018). However, they are governed by ~~a different dynamics (Shapiro and Hill, 1997; Yankovsky and Legg, 2019)~~different dynamics (e.g. Shapiro and Hill, 1997; Yankovsky and Legg, 2019).

This work adds a new dimension of complexity to existing studies by investigating how the net sinking in the North Atlantic changes seasonally and regionally. Despite the promising first results of the Overturning in the Subpolar North Atlantic

Program-OSNAP (Lozier et al., 2017; Kornei, 2018; Holliday et al., 2018; Lozier et al., 2019), the scarcity of measurements below the surface still necessitates the use of numerical models to provide more insight into the spatio-temporal variability of sinking and to grasp the physical processes behind its dynamics. To this end, we use an ocean-only eddy-resolving numerical simulation with a nominal resolution of 0.1° under a repeated climatological annual atmospheric forcing, not adding ~~even more complexity~~ the additional complexity of historical variations (e.g. variations at inter-annual or inter-decadal scales) in surface forcing. Since the degree of buoyancy loss, the topographic configuration, and the oceanic circulation differ among the North Atlantic sub-basins, a complex repartitioning of sinking is anticipated. Therefore we evaluate separately the seasonality and the distribution of sinking at different spatial scales including the marginal seas and overflow areas in the basin. In addition, the connection between sinking and the AMOC is addressed throughout the paper.

The remainder of this paper is structured as follows: in Sect. 2 we introduce the numerical simulation and assess the ability of the model to reproduce a realistic AMOC; in Sect. 3 we consider the main characteristics and the seasonal variability of sinking in the entire subpolar North Atlantic; in Sect. 4 we evaluate similarities and differences between sinking in the marginal seas, overflow regions and mid-latitude seas of the subpolar North Atlantic based on their different bathymetric profiles and driving local dynamical processes; in Sect. 5 we show that in our simulation the connection between sinking variations and the AMOC changes fades when the dominant seasonal signal is removed. To conclude, in Sect. 6 we summarize and discuss the most significant findings.

2 Model data & methods

The model set up is based on a configuration of the Parallel Ocean Program model (POP) (Maltrud et al., 2008; Smith et al., 2010). This model solves the primitive equations on a tri-polar curvilinear grid with a nominal horizontal resolution of 0.1° at the equator and 42 z-layers in the vertical down to a depth of 6000 m. The vertical resolution ranges from 10 m at the surface to 250 m for the deepest layers. The bottom topography is described by partial bottom cells (Adcroft et al., 1997). The atmospheric forcing fields (wind, heat fluxes and precipitation) are applied by repeating a prescribed annual cycle from the Coordinated Ocean Reference Experiment (CORE) forcing dataset (Large and Yeager, 2004). Observed river run-off fields are also included. Table 1 shows the value of some key model parameters. The simulation analyzed here is a subset of a longer control run already employed by Brunnabend and Dijkstra (2017) — see the latter for more details on this simulation.

2.1 Model data & general performance

We use 15 years of three-dimensional monthly-mean fields of velocity, potential density, temperature and salinity for our analysis. Other two-dimensional variables such as bottom depth, the area and volume of grid cells and monthly-mean fields of mixed layer depth are also utilized. Since this study focuses on the seasonal time scale, and because the forcing is annually repeated, 15 years is sufficient to provide robust results. The period selected, corresponding to years 260-274 in the simulation time frame, is chosen well after the spin-up years. We note that inter-annual and larger time scales of variability are not included in our prescribed repeated annual forcing. This does not alter the validity of our analysis at seasonal scales since the annual

Table 1. Summary of POP model key parameters used in the simulation (see Maltrud et al. (2010); Weijer et al. (2012); Brunnabend and Dijkstra (2017) for details)

Parameter	Value
Horizontal resolution	0.1 deg at the equator
Vertical resolution	42 non-equidistant z-levels. From 10 m (surface) to 250 m (deepest)
Horizontal dissipation (momentum)	Bi-harmonic viscosity and diffusion $\propto \mathrm{grid\,size}^3$. At the equator $\nu_0 = -90\,\mathrm{m}^4/\mathrm{s}$
Horizontal dissipation (tracers)	Bi-harmonic viscosity and diffusion $\propto \mathrm{grid\,size}^3$. At the equator $k_0 = -30\,\mathrm{m}^4/\mathrm{s}$
Vertical Mixing (K-profile)	$0.1\,\mathrm{m}^2/\mathrm{s}$ to solve gravitational instabilities
Background vertical tracer diffusion	From $10^{-5}\,\mathrm{m}^2/\mathrm{s}$ (surface) to $10^{-4}\,\mathrm{m}^2/\mathrm{s}$ (depth)

cycle of winds and heat fluxes are dominant. Maps with mean ocean currents for the North Atlantic Ocean at depths of 5 m and 1139 m (Fig. S1) show realistic strength and location of the Gulf Stream and other subpolar boundary currents, taking into account the resolution of the model. Previous work using the same model in a similar set-up found a well-represented distribution of currents, kinetic energy and water-mass properties at basin scale (Maltrud et al., 2010; Weijer et al., 2012; Brunnabend and Dijkstra, 2017). Moreover the modelled mixed layer depth qualitatively matches the spatial pattern derived from ARGO floats (Våge et al., 2009; Holte et al., 2017), where the areas of deepest convection are found in the south-west Labrador Sea, in the Greenland Sea and around the Iceland-Scotland Ridge. However the modelled data shows some delay in reaching the deepest mixed layer depth in the Labrador Sea (March against April) and tends to overestimate the observed mean values in some areas (compare Fig. S2 with Fig. S3). We partly attribute this to the use of repeated normal-year forcing conditions for wind and heat fluxes. We note also that the spatial coverage by ARGO floats is still scarce and hence gridded fields are coarser than model data. Besides, both results are sensitive to the algorithm used to compute the mixed layer depth (de Boyer Montégut et al., 2004).

2.2 Overturning streamfunction

The overturning streamfunction (ψ_o) is a measure of the AMOC strength. With this metric northward and southward flows can be identified, as well as the depth where the transport reaches its maximum. ψ_o is determined from the vertical integral of the zonally integrated meridional velocity at the southern boundary of our domain, and the running meridional integral of the zonally integrated vertical velocity, i.e.:

$$\psi_\mathrm{o}(y,z,t) = -\int_{x_w}^{x_e}\int_{H(x',y')}^{z} v(x',y_0,z',t)\,dz'dx' + \int_{y_0}^{y}\int_{x_w}^{x_e} w(x',y',z',t)\,dx'dy' \tag{1}$$

where $v(x',y_0,z',t)$ and $w(x',y',z',t)$ are the meridional and vertical ocean velocity components, y_0 is latitude of the southern boundary (selected at $y_0 = 25^\circ$N), $H(x',y')$ is the ocean bottom depth and x_w and x_e are the western and eastern

boundaries of the North Atlantic Ocean respectively (Fig. 1A). The model simulation analyzed here yields a maximum time-averaged overturning streamfunction of 25.6 Sv near 35°N, whereas the modelled ψ_o at the RAPID array location (26°N) shows a maximum time-average transport of 22.3 ± 1.9 Sv (Fig. 1B, blue line). This value is within the interval of uncertainty of the annual mean RAPID array observations prior to 2008, 18.8 ± 4.3 Sv (Cunningham et al., 2007; Kanzow et al., 2010), and slightly larger than observations if we consider a longer RAPID period (April 2004-January 2017) with 17.0 ± 1.9 Sv (the uncertainty is the standard deviation). Recent model-based results from Sinha et al. (2018) indicate that the RAPID array may be underestimating the transport by about 1.5 Sv, due to structural errors in the array set-up. Not surprisingly, our simulation is less successful in reproducing the range of variability of annual averages at the RAPID array (April 2004-January 2017), underestimating this variability by almost 5 Sv, with a range of 3.2 Sv against the measured 7.9 Sv (Smeed et al., 2014, 2018). This underestimation is likely due to the use of seasonal mean wind forcing conditions, where the atmospheric high-frequency variability has been partially filtered. Finally, the depth of the maximum time-averaged ψ_o is 1139 m (Fig. 1A), very close to the depth found at the RAPID array location, at about 1100 m (Smeed et al., 2014, 2018). At 45°N (red line in Fig. 1B), the modelled AMOC is around 8 Sv weaker than at the RAPID array location but presents a more pronounced seasonal cycle (around 10 Sv), with the maximum in August and the minimum in February. Results from two dedicated campaigns in different years covering the OSNAP sections ($\sim 50^\circ - 60^\circ$N) provided a similar range of variability for ψ_o, $\sim 10-20$ Sv (Holliday et al., 2018). The recent first assessment of the OSNAP observations by Lozier et al. (2019) yields a mean estimate of the ψ_o that is smaller than our mean ψ_o at 45°N (around 6 Sv smaller) but that compares well with our mean modeled results at 55°N (8.0 ± 0.7 Sv versus 8.1 ± 2.4 Sv, not shown). The depths of maximum ψ_o are located at around 1000 m for the OSNAP observations and at around 1100 m for our simulation for both 45°N and 55°N. In contrast, their results do not show a clear seasonal signal in the AMOC while our simulation shows a marked seasonality in ψ_o for 45°N (~ 10 Sv) and 55°N (~ 8 Sv). We partly attribute this difference between the observations and our modeled results to the short OSNAP time series (only 21 months, from August 2014 to April 2016), and to the fact that we are using normal forcing conditions with a dominant seasonal signal without high-frequency wind variability. Nevertheless, ~~it can be inferred~~ a stronger transport in summer than in winter can be inferred from the OSNAP observations (Lozier et al., 2019), which is in agreement with our modeled results. Therefore we conclude that our simulation displays an AMOC with reasonable mean transport and variability, and a well-located core in depth.

3 Mean and seasonal characterization of net sinking in the subpolar North Atlantic

~~The AMOC only provides~~ The structure of the AMOC streamfunction (Fig. 1A) indicates that there is a decrease in the amount of transport between the North Atlantic mid-latitudes and the subpolar region that, by mass conservation, must be reflected in the magnitude of the vertical transport. However, such figures only provide a two-dimensional view of the overturning circulation in the subpolar North Atlantic. In this study we analyze the complex full structure of the circulation by characterizing spatial and seasonal variations in the sinking. In Sect. 3.1 we present the spatial distribution of modelled vertical velocities, which we use to compute the net vertical transport for the subpolar North Atlantic Ocean, its seasonal variability and its vertical

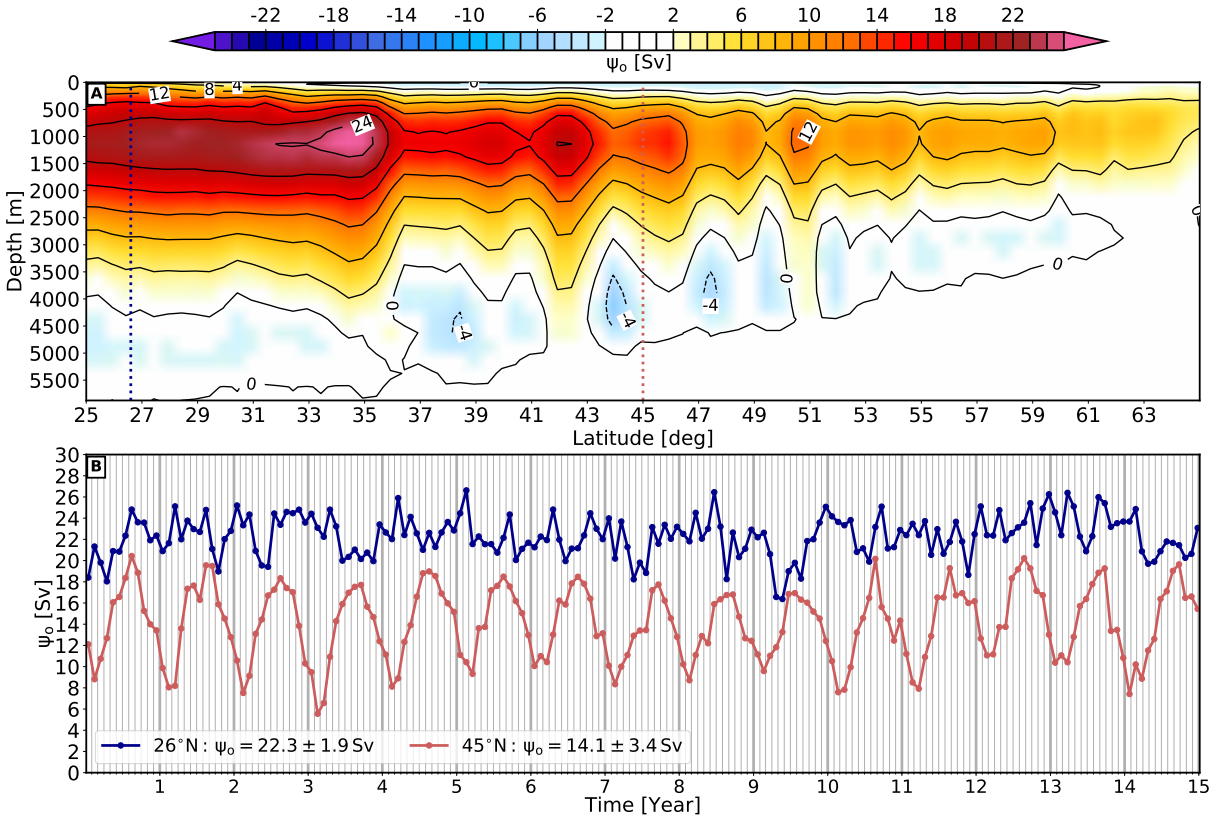

Figure 1. (A) 15-year average (years 260-274) overturning streamfunction, $\psi_o(y, z)$, for the North Atlantic Ocean. (B) Time series of maximum overturning streamfunction at 26°N (blue) and 45°N (red); positions are also indicated by dashed lines in Fig. 1A. $1\,\mathrm{Sv} = 10^6\,\mathrm{m}^3\,\mathrm{s}^{-1}$.

structure. In Sect. 3.2 a distinction in sinking regimes is proposed based on the differences in the net vertical transport between the near-shelf and the interior regions. To conclude this Section, we discuss our results in light of earlier studies.

3.1 Vertical structure of sinking

A map of the mean distribution of the maximum vertical velocities ($\overline{w}_{\max}$, the sign is conserved) obtained from the monthly mean fields in the North Atlantic (Fig. 2A) shows a spatial pattern characterized by strong velocities mostly confined to the boundaries. This is in line with results from idealized models (Spall and Pickart, 2001; Spall, 2004; Straneo, 2006; Spall, 2010; Georgiou et al., 2019; Brüggemann and Katsman, 2019) and global ocean models (Katsman et al., 2018). $\overline{w}_{\max}$ may reach values of over 150 $\mathrm{m\,day}^{-1}$, in good agreement with glider-based observations (Frajka-Williams et al., 2011). Fig. 2B shows the depth at which the velocities are most intense; the black points mark where $|\overline{w}_{\max}|$ is larger than 80 $\mathrm{m\,day}^{-1}$. Most of the strong vertical velocities are found at a depth around 1000 meters (black contour in Fig. 2A) close to the boundaries. ~~However, there are some exceptions, such as near the Flemish Cap and in the interior of the Greenland and Norwegian Seas. There, strong vertical velocities are found farther offshore~~These strong vertical velocities cannot be considered as noise

since they show a coherent spatial pattern along the bathymetric contours and their standard deviation is several times smaller (square root of variance shown in Fig. 2C, about $30\,\mathrm{m\,day^{-1}}$) than their mean value. At some locations, alternating patterns of upward and downward motions are found (Fig. 2A, south-east of Greenland). ~~Possibly~~As shown later, water is forced to move up and down there due to the dynamical restrictions imposed by the full vorticity balance on topographic slopes ~~(see e.g., Spall, 2010; Brüggemann and Katsman, 2019)~~(see e.g., Spall, 2010). The positive and negative ~~alternation near~~ alternations offshore of the Flemish Cap ~~needs to~~ and in the interior of Greenland and Norwegian Seas must have a different cause~~, such as eddy-induced vertical velocities~~. In the case of the Flemish Cap, they occur at the edges of eddies (Fig. S4) and the depth of largest sinking is below 2000 m (Fig. 2B, also in the interior of Norwegian and Greenland Seas), which indicates these eddies are deep and possibly have a strong barotropic component. Indeed, the high variance of vertical velocities ~~$\sigma^2(w)$ near~~ in the surroundings of the Flemish Cap ($\sigma^2(w)$) is a reflection of the existence of an active eddy field throughout the year (Fig. 2C). Also the subsurface EKE shows this signal (Fig. ~~S4). Note that the depth of $\overline{w}_{\max}$ in this region is much larger than 1000 m, which suggests the presence of deep eddies with a strong barotropic component.~~ S5).

To assess the magnitude and the depth at which the near-boundary sinking occurs, we sum the local vertical transport for the entire subpolar North Atlantic. First, we calculate the vertical transport for all model grid points and for every depth as $W(x,y,z,t) = w(x,y,z,t)A(x,y)$, where $A(x,y)$ is the area of the grid cell, which depends on its location (x,y) in our curvilinear grid. Second, we sum W over the horizontal domain ~~of study defined~~ shown in Fig. 2. We will refer to this net vertical transport as W_Σ for simplicity. The vertical profile of W_Σ is shown in Fig. 3A. Large negative values of W_Σ are found between 500-2700 m, with the strongest downward transport located at a depth of 1139 m. By mass conservation we expect that W_Σ in our domain will be closely related to the transport at the southern boundary of the domain ($45°$N) since the North Atlantic Current is the dominant feature in the basin, although some mass contribution from the Arctic Ocean at $75°$N and through the Davis Strait can be expected (Rudels et al., 2005; Azetsu-Scott et al., 2012). A comparison between time series of minimum W_Σ and the maximum ψ_o (Fig. 1B) yields an excellent agreement in magnitude: $14.1 \pm 3.4\,\mathrm{Sv}$ against $-13.6 \pm 4.1\,\mathrm{Sv}$ (Fig. 1B and Fig. 3A). If we compare the reversed time series of ψ_o at $45°\,\mathrm{N}$ (solid red line in Fig. 3B) with the time series of W_Σ at the depth of minimum W_Σ (solid purple line) it is clear that also the seasonal signal matches, with the minimum W_Σ in summer (August) and the maximum in winter (February). The broadest range of variability (maximum minus minimum) is around 12 Sv in both time series at $\sim$1100 m depth. If we repeat the comparison after removing the seasonal signal from both time series (dashed lines in Fig. 3B) the high correlation persists (> 0.9), but with a reduced maximum range of variability of 5 Sv.

3.2 Variation of sinking according to distance from the ~~coast~~shelf

In order to quantify how much sinking takes place near the boundaries versus in the interior we have first classified all ocean grid points within the study area (domain in Fig. 2) according to their distance to the nearest ~~land point~~ bathymetric contour of 50 m of depth, C_{50} (inset map in Fig. 4); Next, we have accumulated W starting from ~~the coast~~ C_{50} towards the interior at the depth where W_Σ (note the added spatial dependence) is at its minimum (at 1139 m, Fig. 3A). On average (dashed black line

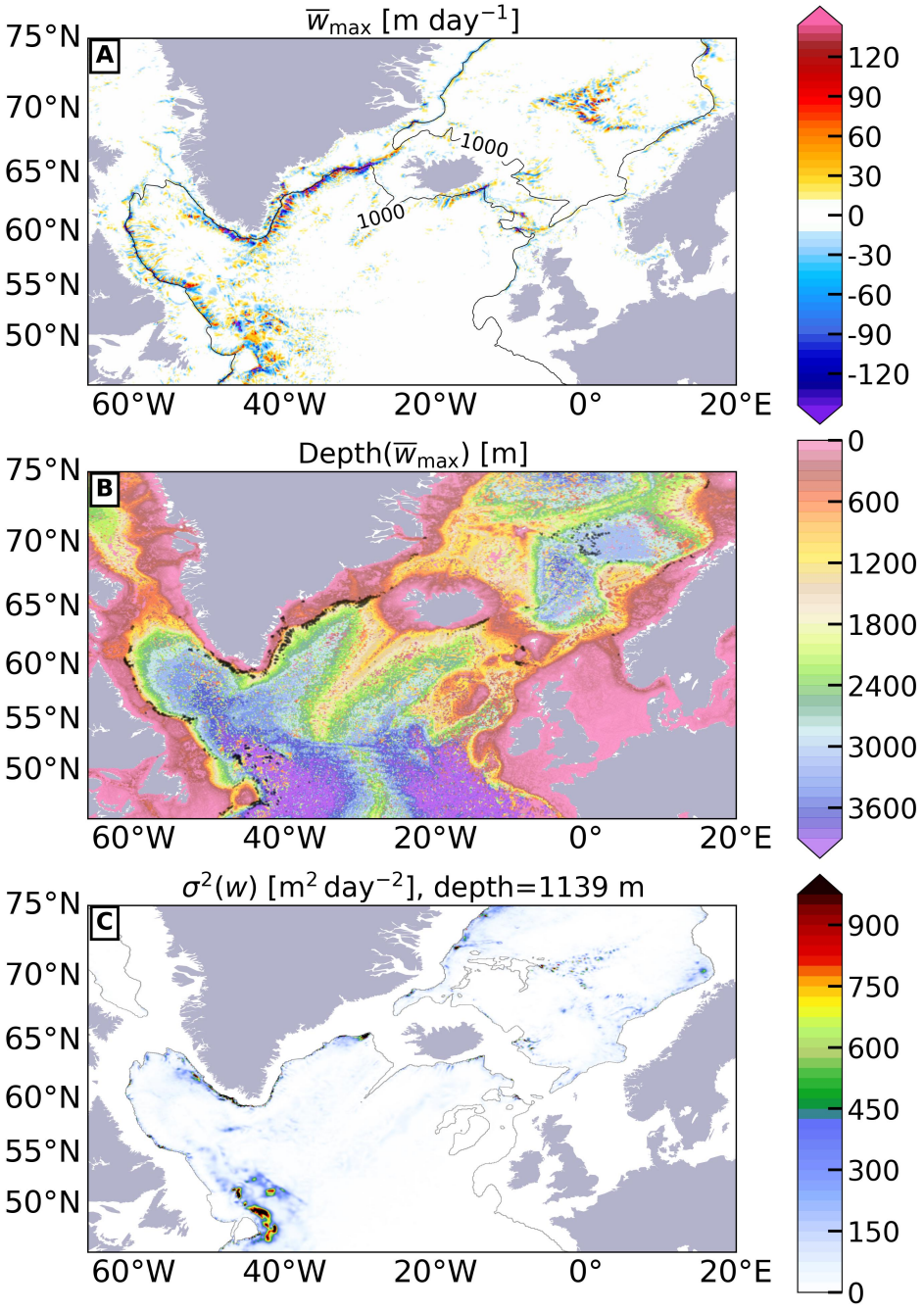

Figure 2. (A) 15-year maximum mean vertical velocity ($\overline{w}_{\max}$) for the North Atlantic Ocean. Contour lines denote the two longest 1000 m bathymetric features, which are separated by the Denmark Strait and the Iceland-Scotland ridge. (B) Depth of $\overline{w}_{\max}$ plotted in (A). Black dots mark those grid cells where $|\overline{w}_{\max}|$ is larger than 80 $\mathrm{m\,day^{-1}}$. (C) 15-year variance of vertical velocity ($\sigma^2(w)$) at a depth of 1139 m. This depth corresponds to the depth at which the vertical transport associated with the AMOC peaks.

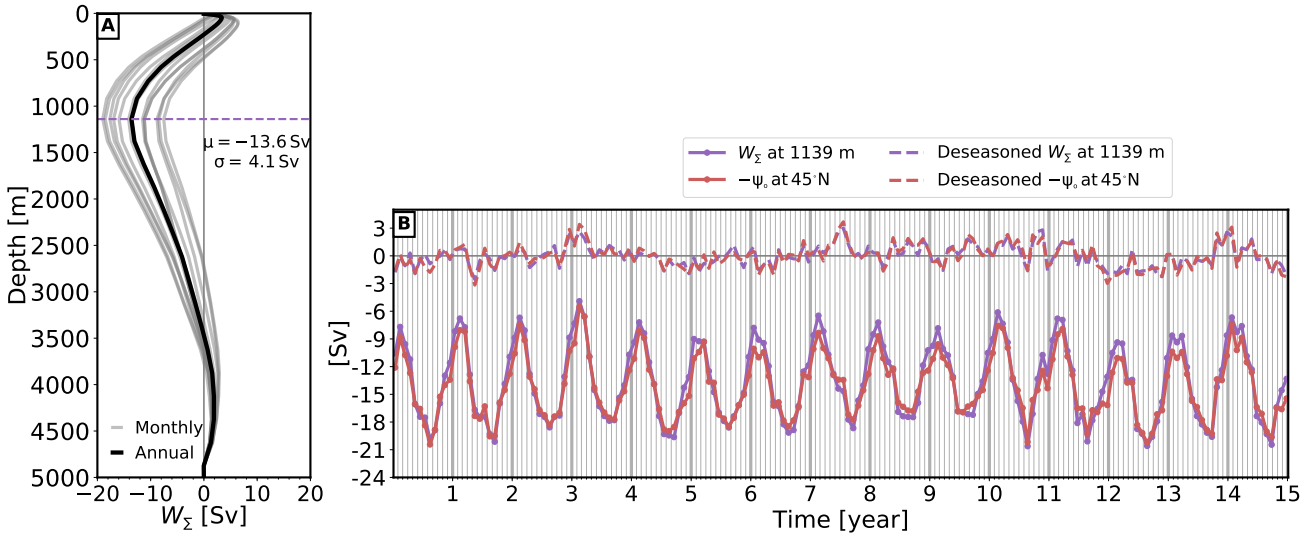

Figure 3. (A) Mean profile of the net vertical transport (W_Σ) for the region of study [66° W − 20° E, 45° N − 75° N]. The annual mean profile is shown by a thick black line; as the monthly climatology is indicated by gray lines. Mean and standard deviation (μ, σ) are given in the legend; the depth of largest sinking (1139 m) is indicated with a horizontal purple line. (B) Time series of W_Σ at 1139 m (purple lines, in Sv) compared to the reversed time series of maximum ψ_o (Figure 1B) at 45° N (red lines, in Sv). Solid lines include the seasonality while dashed lines do not include the seasonal signal (see legend). The Pearson correlation coefficient between both time series is over 0.9 for both cases.

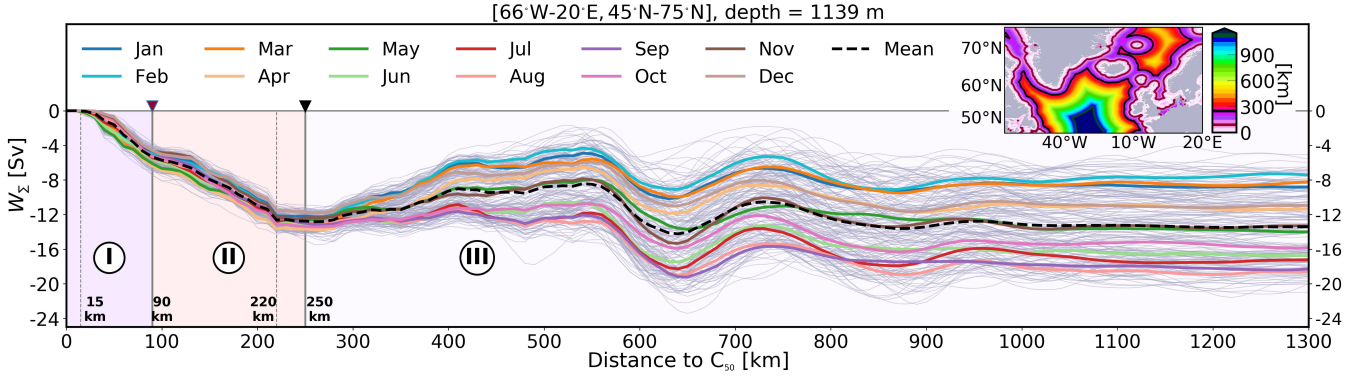

Figure 4. Cumulative net vertical transport (W_Σ) at a depth of 1139 m (in Sv) as a function of the distance from the ~~coast defined in the~~ bathymetric contour of 50 m depth referred to as C_{50} (inset map ~~(~~in ~~km~~Fig. 4). If the grid cell bathymetry is shallower no value is added. The dashed black line shows the annual mean. Monthly values of the 15-year simulation are shown in light gray, colored lines indicate the monthly climatology. The regimes of sinking are indicated by roman numbers **I-II-III**, and the separation lines between them are also denoted by a brown and a black triangle and by contours in the same color in the inset figure.

in Fig. 4), −12 of −13.6 Sv (∼ 90%) of W_Σ occurs in the first ~~290~~ 250 km off the ~~coast~~C_{50}. A first assessment suggests the existence of three different sinking regimes according to the distance to ~~the coast~~ C_{50} (indicated as regimes **I-II-III** in Fig. 4):

I *Distance* ~~≤ 110~~ ≤ 90 km. This region presents the largest increase in sinking with respect to the distance to ~~the coast~~C_{50}. It displays a small seasonal variation of less than 2 Sv. The minimum accumulated W_Σ at 1139 m occurs in ~~May (dark green~~ April (light orange line) and is around ~~-7~~ -6 Sv over a distance of ~~~ 60~~ ~ 70 km.

II *Distance between* ~~$110 - 290$~~$90 - 250$ km. The accumulated W_Σ in this section remains intense though smaller than in regime **I** with ~~~ -5 Sv over 100~~ ~ -7 Sv over 130 km. The magnitude of accumulated W_Σ increases until about 220 km from ~~the coast~~C_{50}. Between 220 and 290 km the curve flattens, indicating that no additional sinking occurs or that it is locally compensated by rising waters. Seasonal variations are slightly larger than for ~~the~~ regime **I**, with values over 3 Sv between the months of April (light orange line) and December (light brown line).

III *Distance* ~~> 290~~ > 250 km. Beyond ~~290 km from the coast~~ 250 km from C_{50} the trend in accumulated W_Σ can revert completely with respect to regimes **I** and **II** depending on the season. During winter months, there is a net positive accumulated W_Σ (i.e. net upwelling) between 290 and 750 km~~. During~~ ; during summer months a negative accumulated W_Σ tends to occur. As a result, the final amount of accumulated W_Σ displays a large seasonal variability, with deviations of up to 11 Sv between winter and summer months at a distance of over 750 km from ~~the coast~~C_{50}. The annual mean of accumulated W_Σ varies little with distance from the coast in this regime (only $1-2$ Sv, compare the black dashed line in Fig. 4 at 290 km and at 1000 km). The seasonal variations strongly affect the accumulated W_Σ in some specific months (e.g. in February -light blue line- or in August -pink line-), yielding changes in the accumulated W_Σ of up to 50% of what is seen in the first 290 km off ~~the coast~~C_{50}.

It is hypothesized that these three sinking regimes reflect the effect of different processes contributing to the sinking. This is illustrated in Fig. 5, by means of a time-mean vertical cross-section of the horizontal and vertical velocity field (see inset panel A). First, there is sinking of waters between 500 and 2000 m along the Greenland shelf-slope all year round (black arrows on the right hand of panels A-D). This sinking is connected with regimes **I** and **II** (Fig. 4), and occurs within the boundary current (blue shading) below the mixed layer depth (light green line). Most of this sinking is constrained to a distance around 200 km off ~~the coast~~ C_{50} in a region where isopycnals are tilted, and displays little seasonal variation. Second, there is a permanent anticyclonic eddy of about 200 km of diameter at 1000-1250 km south of the tip of Greenland that extends from the surface to a depth below 4000 m (shading), and generates both intense positive and negative vertical velocities at its flank (black arrows). This pattern of interior ~~eddy-induced~~ rising/sinking of waters ~~yields~~ yield a small net annual mean vertical transport over the entire basin but significant seasonal variability, which is reflected in sinking regime **III** (Fig. 4).

The boundary sinking found by Katsman et al. (2018) in a global ocean model and here characterized by regimes **I** and **II** is captured by the ageostrophic theory and in idealized models (Spall, 2010; Brüggemann and Katsman, 2019; Georgiou et al., 2019)~~, which explained its basic features in terms of the vorticity balance~~. Thus, the narrow band of sinking closer to ~~the coast~~ C_{50} represented by the sinking regime **I** is characterized by the preeminent role of the topographically induced dissipation, while the sinking farther offshore represented by regime **II** is presumably largely driven by the presence of eddies near the boundary. Indeed, the amount of sinking is governed by eddy-advection in the cross-shore direction (Georgiou et al., 2019), so

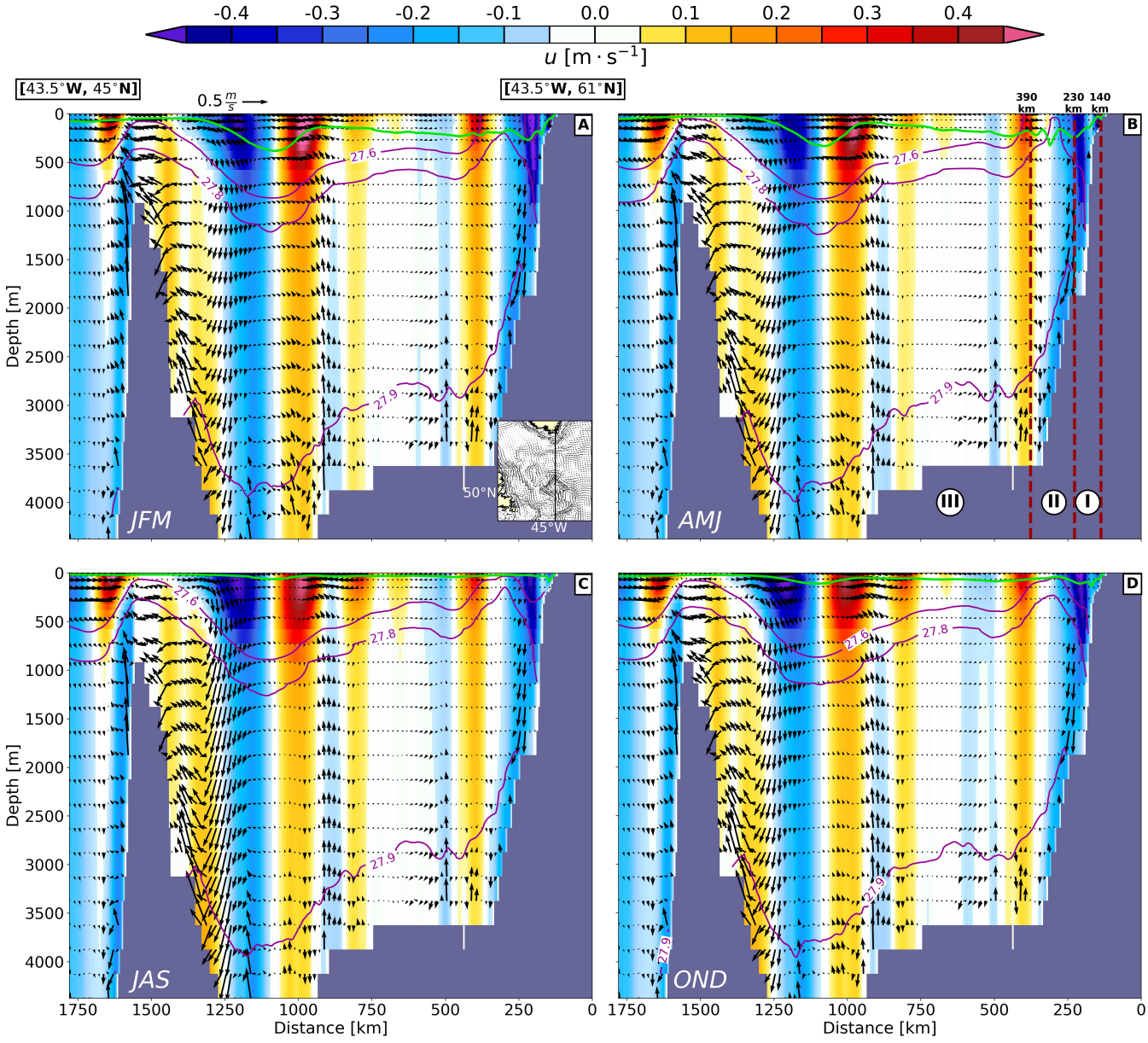

Figure 5. 15-year climatology of the velocity field at a cross-section between the southern tip of Greenland and the southern limit of the study area (see inset in panel A, main surface currents denoted by black arrows). Each panel represents a seasonal average: (A) JFM (January-February-March); (B) AMJ (April-May-June); (C) JAS (July-August-September); OND (October-November-December). The shading shows the u component of velocity (units in $\mathrm{m\,s^{-1}}$); black arrows are velocity vectors constructed as $(v,\, 1000 \cdot w)$. For clarity arrows are shown for 1 of every 3 horizontal grid points at certain depths. The green line depicts the seasonal mean mixed layer depth (in m), the black contours denote the seasonal potential density anomaly, $\sigma_\rho = \rho - 1000$, for selected values. The limits of the proposed sinking regimes (**I-II-III**) are sketched in panel B through vertical dark red dashed lines.

it is not surprising that this region presents a larger seasonal signal compared to the one described by regime **I** (Fig. 4, see also the patches of strong EKE near the southern tip of Greenland in Fig. ~~S4~~S5).

Spall and Pickart (2001) derived a simple expression to estimate the magnitude of meridional overturning ($\mathrm{M_B}$) —or by mass conservation, the downward vertical transport W_Σ— near the boundary for a situation with a deep mixed layer:

$$\mathrm{M_B} = W_\Sigma = \frac{g\Delta\rho_B h^2}{2\rho_0 f}, \tag{2}$$

where the amount of W_Σ is proportional to the square of the mixed layer depth (h) and to along-shore differences in potential density ($\Delta\rho_B$) —g is the Earth's surface gravity, f the Coriolis parameter and ρ_0 a reference density—. Although ~~Brüggemann and Katsman (2019) have shown that~~ Eq. (2) is not formally correct when the mixed layer depth is shallow (as is the case here), Katsman et al. (2018) demonstrated that the relationship yields reasonable results in a realistic global ocean model when the mixed layer depth (h) is substituted by half of the depth of largest sinking and the along-shore density change ($\Delta\rho_B$, which for this situation depends on depth) by its depth average. ~~The~~ Eq. (2) indicates that the net vertical transport is among others controlled by the local along-shore density gradient ($\Delta\rho_B$), that is, a negative W_Σ is associated with a rise in the isopycnals along the boundary current (or equivalently, by the densification of waters at a given depth). This proportionality of the boundary sinking to the density gradient along the boundary was also pointed out by Straneo (2006) in her two-layer model approach. This connection is also suggested here by the strong vertical velocities in the boundaries (Fig. 2A-B) and by the upward displacement of the isopycnals between the eastern (south-east of Iceland) and the western (south-west of Greenland) sides of the basin (see the mean depth of isopycnals of $\sigma_\rho = 27.75$ and $27.8\ \mathrm{kg\cdot m^{-3}}$ in Fig. ~~S5A-B~~S6A-B). Indeed this along-shore tilting is always present and has its maximum in spring (Fig. ~~S6~~S7).

Apart from the isopycnal tilting ~~, Brüggemann and Katsman (2019)~~ in alongshore direction, Brüggemann and Katsman (2019); Georgiou that the cross-shore density gradients also contribute to the budget of boundary sinking since, as eddies arise from baroclinic instabilities, they try to flatten the isopycnals. This can be accompanied by strong vertical velocities and, hence, more sinking (see for example the cross-shore density gradient in Fig. 5, where the isopycnal of $\sigma_\rho = 27.8\ \mathrm{kg\cdot m^{-3}}$ is tilted within the boundary current near the southern tip of Greenland).

Finally, the sinking in regime **III** is related to those processes that develop away from the shelf and far from the core of the boundary current. ~~Therefore eddies are more likely to drive this series of positive and negative events of vertical transport~~ In this case, strong vertical velocities appear at the edge of interior eddies, which are governed by a different dynamics (Fig. ~~2A and Fig.~~ 5). The major role of such quasi-permanent eddies is supported by the marked fluctuations between 300 and 1000 km in Fig. 4, the large interior eddy in Fig. 5 and the vigorous EKE field ~~around~~ in the interior of the Newfoundland Basin, near the Flemish Cap (Fig. S4 and Fig. S5).

4 Regional distribution of net vertical transport

The overall view of net vertical transport (W_Σ) in the subpolar North Atlantic presented in the Sect. 3 may not be valid at regional scales, since the bathymetric configuration, the ocean circulation and water-mass properties differ between the different seas. Moreover, the dynamics of overflows are different from those governing the near-boundary sinking induced by the buoyancy loss of a boundary current. In order to assess and understand these expected spatial variations we divide the subpolar North Atlantic in eight well-established regions (see Fig. 6), which for discussion purposes can be grouped into three more general sets: marginal seas (Labrador, Irminger, Greenland and Norwegian Seas -Sect. 4.1-), overflow regions (Denmark Strait and Iceland-Scotland Ridge -Sect. 4.2-) and mid-latitude seas (Newfoundland and Rockall, -Sect. 4.3-). In the remainder of this Section we will describe the following properties associated to W_Σ for these three groups of regions:

(i) The time-mean W_Σ at the depth of minimum W_Σ (hereinafter this depth is defined as $z_{\min}$).

(ii) The seasonal variability of W_Σ and $z_{\min}$.

(iii) The signal to noise ratio (SNR), defined as $\mathrm{SNR} = \left|\frac{\mu}{\sigma}\right|$ (μ = time-mean of W_Σ at $z_{\min}$, σ = standard deviation of W_Σ at $z_{\min}$), a high value ($\mathrm{SNR} > 1$) indicates that μ is relatively large compared to σ, whereas a small value ($\mathrm{SNR} < 1$) denotes a signal with a large temporal variability compared to the mean—although it does not necessarily imply a well-defined seasonal signal as SNR does not yield any information on its periodicity—.

(iv) The regimes of sinking that can be identified.

In Sect. 4.4, a further evaluation of the sinking characteristics of the Labrador Sea, Irminger Sea and Newfoundland regions (which represent about $2/3$ of net sinking in the subpolar North Atlantic and cover all three types of regions) is provided.

4.1 Marginal seas

Vertical profiles of W_Σ for the marginal seas (Fig. 7A-D) indicate that on average the Labrador Sea contributes about twice as much to the sinking as the other three marginal seas combined (~~−4.04 Sv against −2.1~~ −4.02 Sv against −1.57 Sv), yielding a total mean W_Σ of ~~−6.14~~ −5.59 Sv in the marginal seas (see μ in Fig. 7A-D, and Table 2 for a complete summary; notice the different value of $z_{\min}$ for each region). This contribution from the Labrador Sea is larger than the -1.4 Sv derived by Katsman et al. (2018) using a coarser ocean model (ORCA025). This is probably due to the improved ability of higher-resolution models to resolve the eddy activity and ageostrophic processes near the boundary (Georgiou et al., 2019; Brüggemann and Katsman, 2019), which gives rise to stronger vertical transports. It is also larger than the -1 Sv estimated by Pickart and Spall (2007) using the World Ocean Circulation Experiment (WOCE) AR7W line data and the -1.2 Sv estimated from Argo floats by Holte and Straneo (2017) at a shallower depth (around 800 m). This substantial difference may be due to the scarcity of observations. Interestingly the value of $z_{\min}$ for the Labrador Sea matches the one previously shown in Fig. 3A for the whole basin (1139 m). The Greenland Sea also shows a time-mean W_Σ that stays negative during the whole year of about ~~−1.1~~ −1.2 Sv (Fig. 7C), with the minimum W_Σ (largest sinking) occurring in June and the maximum in February (Table 2). ~~It displays a similar vertical~~

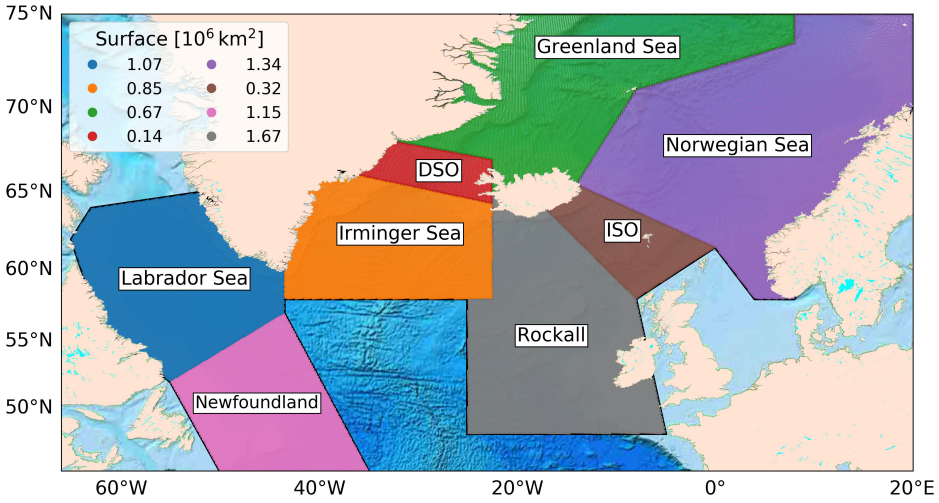

Figure 6. Map of the North Atlantic [66° W − 20° E, 45° N − 75° N] divided into eight regions. DSO and ISO refer to Denmark Strait and Iceland-Scotland Ridge overflow regions respectively. The surface area of each region is shown in the legend in $10^6 \cdot \mathrm{km}^2$.

shape as in the Labrador Sea, although In this case $z_{\min}$ is now located at a depth near 730 m around 80 m, with a quasi-linear decrease in the magnitude of sinking until a depth of 1800 m at which it is nil. The sinking in the Irminger and Norwegian Seas is more variable and depends on the time of the year season, yielding net positive (negative) W_Σ during winter (summer) months (Fig. 7B,D). This yields a smaller annual mean sinking than in the Labrador and Greenland Seas of -0.73 Sv and -0.25 Sv respectivelyfor the Irminger Sea of -0.75 Sv and net upwelling of +0.37 Sv for the Norwegian Sea. A notable difference between the Irminger and Norwegian Seas is the value of $z_{\min}$, which is ~ 470 m for the Norwegian Sea and ~ 1630 m for the Irminger Sea.

The magnitude of the seasonal variability of W_Σ is exhibited in Fig. 8, where the time series of W_Σ at $z_{\min}$ with (solid lines) and without (dashed lines) the seasonal signal are depicted for each region (Fig. 7 and Table 2). It displays a negative W_Σ all year round for the Labrador Sea that varies between -2 Sv (winter) and -5 Sv (late spring/summer). This result for the Labrador Sea qualitatively agrees agrees qualitatively with Holte and Straneo (2017), who also found the strongest sinking in spring (-1.2 Sv) and the weakest sinking in winter (-0.6 Sv). Georgiou et al. (2019) also found this intensification of the sinking during spring in their idealized Labrador Sea model in response to the larger density gradients between the boundary and the interior. The Irminger and Norwegian Seas share a large temporal variability that is reflected in an almost identical elevated standard deviation of ~ 1.1 Sv and 1.4 Sv respectively (Fig. 7B,D), and a seasonal variability of ~ 3 Sv, similar to that found in the Labrador Sea (Fig. 8BS8B,D). For the Irminger Sea, $z_{\min}$ remains constant during the year while for the Norwegian Sea it changes every season with an abrupt deepening in winter when it reaches a depth of ~ 1200 m (horizontal dashed black lines in Fig. 8BS8B,D). Contrarily, the Greenland Sea shows a weak The Greenland Sea also shows some seasonal variability of W_Σ at $z_{\min}$ (0.5 1 Sv, Fig. 8C), but S8C), with the depth of largest sinking shallows shallowing significantly during winter to ~ 100 m (black dashed lines in Fig. 7C), when the strongest sinking occurs. In terms of SNR, the Labrador Sea has a high value of ~ 5,

Table 2. Summary of properties of the sinking shown in Fig. 3A and Fig. 7 for the entire study area (Domain) and all regions defined in Fig. 6. μ denotes the time-mean net vertical transport (W_Σ) at the depth of minimum W_Σ ($z_{\min}$), and σ its the standard deviation. Min and Max denote the months when the minimum and the maximum W_Σ (or equivalently the largest and the smallest sinking) occur respectively. The final column shows the signal to noise ratio (SNR), defined as $\mathrm{SNR} = \left|\frac{\mu}{\sigma}\right|$.

Area	$\mu \pm \sigma$ **[Sv]**	$z_{\min}$	**Min**	**Max**	$\mathrm{SNR} = \left\|\frac{\mu}{\sigma}\right\|$
Domain	-13.6 ± 4.1	1139	August	February	3.3
Labrador Sea	~~-4.04 ± 0.83~~ -4.02 ± 0.83	1139	June	January	4.9
Irminger Sea	~~-0.73 ± 1.13~~ -0.75 ± 1.13	1626	August	March	0.6
Greenland Sea	~~-1.12 ± 0.15~~ -1.19 ± 0.43	~~729~~ 83	~~June~~ January	~~February~~ September	~~7.5~~2.8
Norwegian Sea	~~-0.25 ± 1.08~~ $+0.37 \pm 1.42$	466	~~September~~ August	January	~~0.2~~0.3
Denmark Strait	-2.24 ± 0.28	729	February	August	8
Iceland-Scotland	~~-2.27 ± 0.72~~ -2.75 ± 0.37	~~1139~~ 918	July	~~January~~ February	~~3.1~~7.4
Newfoundland	~~-3.71 ± 1.85~~ -3.82 ± 1.86	2125	June	March	2
Rockall	~~-1.05 ± 0.59~~ -1.58 ± 0.65	1379	August	February	~~1.8~~2.4

1 ~~although smaller~~ ~ 4.8, which is larger than for the Greenland Sea (~~7.5)where the seasonal signal is hardly identifiable~~2.8). On
2 the contrary, the Irminger and Norwegian Seas yield low values of SNR (~~0.6 and 0.2~~ 0.7 and 0.25 respectively, Table 2), which
3 reflect their remarkable seasonal variability (Fig. ~~8B~~S8B,D). The boundary sinking is delayed from the occurrence of deep
4 convection in the interior of subpolar North Atlantic as demonstrated by the fact that the largest boundary sinking in Labrador
5 and Irminger Seas occurs in late spring/summer while the deep convection takes place in late winter/early spring (Fig. S2).

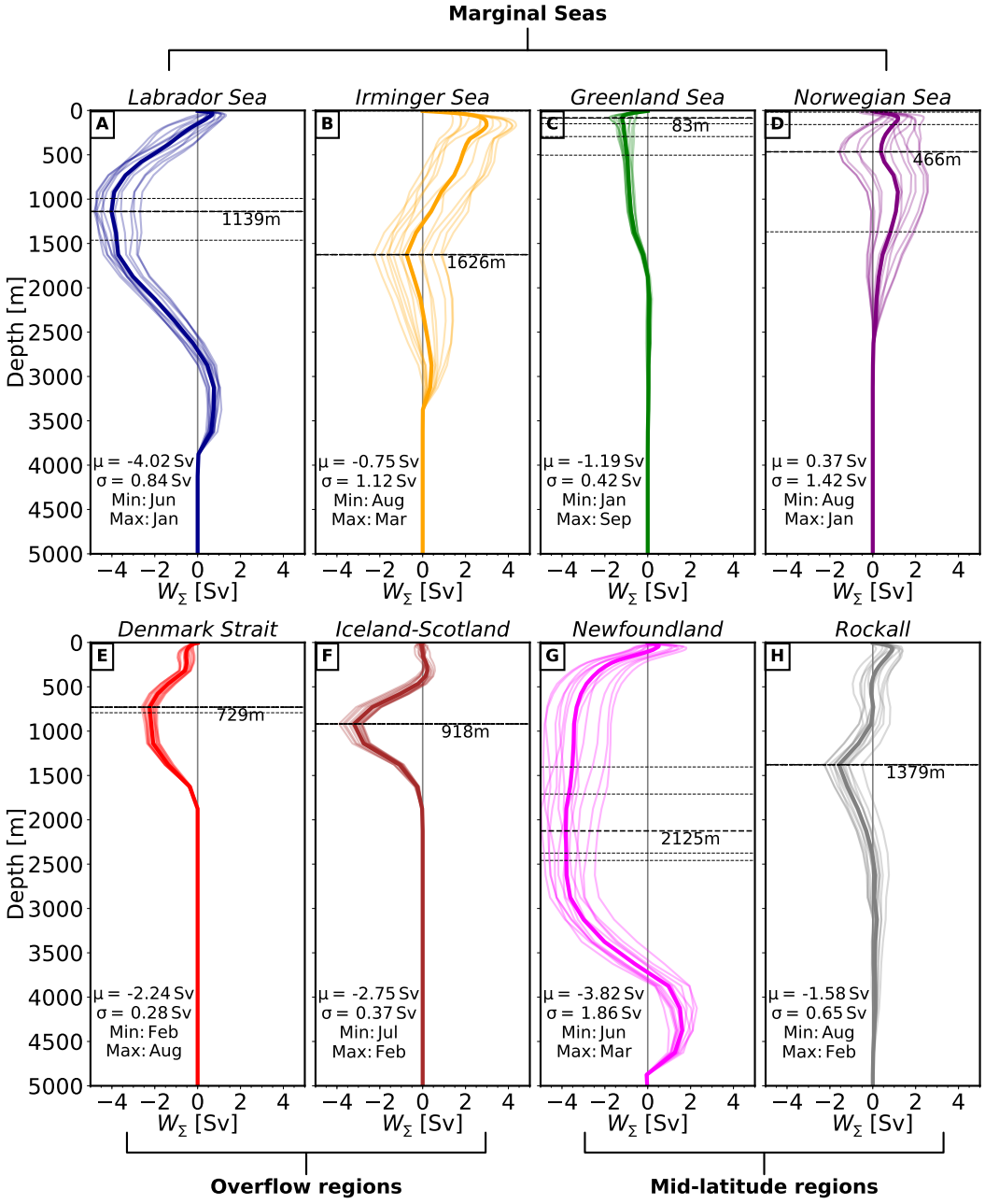

Figure 7. Vertical profile of annual mean (thicker line) and monthly averages (thinner lines) of net vertical transport (W_Σ) for the regions defined in Fig. 6. μ and σ are the climatological mean and standard deviation of W_Σ at the depth of largest sinking (or minimum W_Σ, see legend). $z_{\min}$ is the depth where the largest sinking is found. Max and Min refer to the months with maximum and minimum mean W_Σ (smallest and largest sinking) respectively. Seasonal mean depths of W_Σ are displayed by horizontal black dashed lines.

Next, we evaluate to what extent the sinking regimes proposed in Sect. 3.2 for the entire subpolar North Atlantic are also applicable to the individual regions of interest. To this end we have plotted the accumulated W_Σ from ~~the coast~~ C_{50} to the interior at the depth of largest sinking for each region (Fig. ~~9~~8). Overall, the Labrador, Greenland and Norwegian Seas show the sinking regimes proposed in the Sect. 3.2, with a stronger negative accumulated W_Σ near the slope at distances shorter to C_{50} than 200 km and a small accumulated W_Σ at larger distances. In particular, the Labrador Sea yields an accumulated sinking W_Σ of around -4 Sv in the region covered by the sinking regime **I**, which is larger in magnitude than the ~~-1.5~~ -1 Sv or the -0.5 Sv obtained for the Norwegian and Greenland Seas respectively for the same region (Fig. ~~9A~~8A,C-D). ~~As for the entire subpolar North Atlantic, the~~ The amount of negative accumulated W_Σ in the regime **II** is generally smaller in magnitude in the individual regions: roughly -1.5 Sv for the Labrador Sea~~and~~, -0.5 Sv for Greenland ~~and Norwegian Seas~~ Sea and 0 Sv for Norwegian Sea (Fig. ~~9A~~8A,C-D). Differences between sinking regimes **I** and **II** are subtle but still distinguishable as the slightly larger seasonal variability (up to 2 Sv for the Labrador and Norwegian Seas) and the higher number of oscillations at distances within the regime **II**. In contrast, the Irminger Sea shows a succession of positive/negative accumulated W_Σ over the distances covered by the regimes **I**-**II**, with a negative accumulated W_Σ at ~~290~~ 250 km of around -1 Sv. Depending on the marginal sea considered regime **III** is found from ~~250-300 km off the coast~~200-300 km off C_{50} (shorter for Greenland Sea due to its shallower depth of largest sinking), and it is associated with larger monthly variations of accumulated W_Σ than in regimes **I** and **II**. Some clear examples of this seasonality are exhibited by the Irminger, Norwegian and Labrador Seas with ranges ~~~ 3~~ $\sim 2-3$ Sv (Fig. ~~9A-B~~8A-B,D); the Greenland Sea ~~shows a weaker seasonality (Fig. 9C~~also shows a clear seasonality but weaker (1 Sv) in line with Fig. 8C and Fig. S8C. We note that the pattern of accumulated W_Σ is particularly complex for the Irminger Sea on and near the slope, with positive accumulated W_Σ at a distance to ~~the coast between 100 and 170~~ C_{50} between 90 and 150 km followed by negative accumulated W_Σ between ~~200~~ 210 and 300 km off ~~the coast~~C_{50}. One explanation for that succession of upward/downward moving waters near the boundaries is the uphill/downhill flow along the coast, which is probably linked to the bathymetry (as seen in Fig. 2A, and also supported by a depth of largest sinking that does not vary seasonally in Fig. 7 and by a more dedicated assessment of W in Fig. S9). At distances of more than ~~350 km from the coast~~300 km from C_{50}, the Norwegian and Irminger Seas show a positive accumulated W_Σ during winter yielding a seasonal variation with respect to summer months of ~~2.5 $-$ 3~~ 3 Sv. To summarize, our results confirm that to a large extent the proposed sinking regimes remain applicable to marginal seas, in particular to the Labrador Sea. However, the mentioned differences and similarities among the marginal seas (e.g. their different $z_{\min}$) reveal a complex picture, where the boundaries between the different regimes are not fixed and can shift a few tens of km closer to or farther from ~~the coast. Thus~~C_{50}. That is, sinking regimes are influenced by the local bathymetric features and ~~local~~ processes in each marginal sea.

4.2 Overflow regions

The Denmark Strait and the Iceland-Scotland Ridge are regions where the W_Σ is mainly dominated by the overflow of waters from the Nordic Seas towards the northern subpolar North Atlantic. Fig. 7E-F shows that the mean magnitude of W_Σ is very similar in both regions and amounts to roughly ~~-2.2 Sv~~ -2.2 and -2.7 Sv in Denmark Strait and Iceland-Scotland respectively. Altogether it gives a total value of ~~~ -4.5~~ ~ -5 Sv for overflow waters, which represents at most ~~33~~37% of the total W_Σ at

$z_{\min}$ (compare overflow regions against Domain in Table 2). The outcome from the Denmark Strait is in agreement with the -2.2 Sv estimated by Katsman et al. (2018) for the ORCA025 hindcast (note that they estimated W_Σ in a different area and $z_{\min}$) and 0.25 Sv higher than the transport found by Köhl et al. (2007) in a model simulation. However, these model-based results are about 1 Sv weaker than the hourly observations, which yield -3.2 ± 1.5 Sv (Jochumsen et al., 2017). $z_{\min}$ differs for both regions, and is shallower for the Denmark Strait (729 m) than for Iceland-Scotland (~~1139~~ 918 m). This is related to the respective sill depths in the model.

~~Time series of net vertical transport ($W\ at the depth of minimum$W ($z_{\min}$). This depth varies for each region according to Table 2 (see the plot title). The solid line includes the seasonal cycle; the dashed line shows the deseasoned time series. The seasonal cycle has been subtracted by removing the corresponding climatological monthly mean from every month. Note the different vertical scale of the various plots.~~

The downward transport in the Denmark Strait peaks in February and is weakest in July, which is out of phase with all other regions; the Iceland-Scotland region peaks in ~~August~~ July and is weakest in January (Table 2). Seasonal variability is present in both time series with ranges of 0.6 Sv for the Denmark Strait and ~~2~~ 1 Sv for Iceland-Scotland (which is poorly defined in some specific years) at their respective $z_{\min}$ (solid lines in Fig. ~~8E-F~~S8E-F, and Table 2). Besides this depth shows larger seasonal variations in Iceland-Scotland than in the Denmark Strait (black horizontal dashed lines in Fig. 7E-F). The seasonal signal is smaller in the Denmark Strait than in other basins, with differences between winter and summer (Fig. ~~8E~~S8E) likely due to fluctuations of the overflow plume (Jochumsen et al., 2017; Håvik et al., 2017), which has an observed reduced transport in summer. As other high-resolution models, this model simulation tends to overestimate seasonal changes of overflow waters through the Denmark Strait: observations indicate a seasonal signal of only around 0.05 Sv (Jochumsen et al., 2012). Moreover, sinking in Iceland-Scotland displays slightly larger fluctuations than in the Denmark Strait (~~SNR = 3.1~~ SNR = 7.4 against SNR = 8). This can be explained by its larger extent, ~~covering not only the ridge itself but also the surroundings, where both eddy-induced and near-boundary sinking may exist~~which in this case covers two sills: one near Iceland and another closer to Scotland.

More differences between the Denmark Strait and the Iceland-Scotland regions ~~are obvious~~ become apparent from Fig. ~~9E-F~~ 8E-F where the time-mean accumulated W_Σ is plotted versus the distance to ~~the coast~~C_{50}. The positive and negative accumulated W_Σ in the Denmark Strait over the first 250 km off ~~the coast~~ C_{50} (Fig. ~~9E~~8E) reflect waters moving southward from the Nordic Seas that first flow up and then down over the sill. This is illustrated by the deepening of the isopycnal in Fig. ~~S5C~~ S6C after crossing the Denmark Strait ~~.~~and demonstrated in Fig. 9, in which the Denmark Strait region has been divided in two parts of similar size on either side of the sill (green triangle in Fig. 9A): one that mainly contains the upward movement of waters as they approach the sill (DSO ↑) and another that contains the downward movement of waters after crossing the sill (DSO ↓). As a result, this up/down transport is clearly reflected in Fig. 9B-C, with the strongest upwelling (+1 Sv) located at a depth of 579 m, and the strongest sinking (−3 Sv) is found at 729 m. The difference between DSO ↑ and DSO ↓ accounts for the near 2 Sv of net sinking found in this region. Furthermore, the accumulated vertical transport with respect to the distance to the sill at the respective depths of strongest upwelling and sinking show that the most important contributions occur within the first 150 km off the sill.

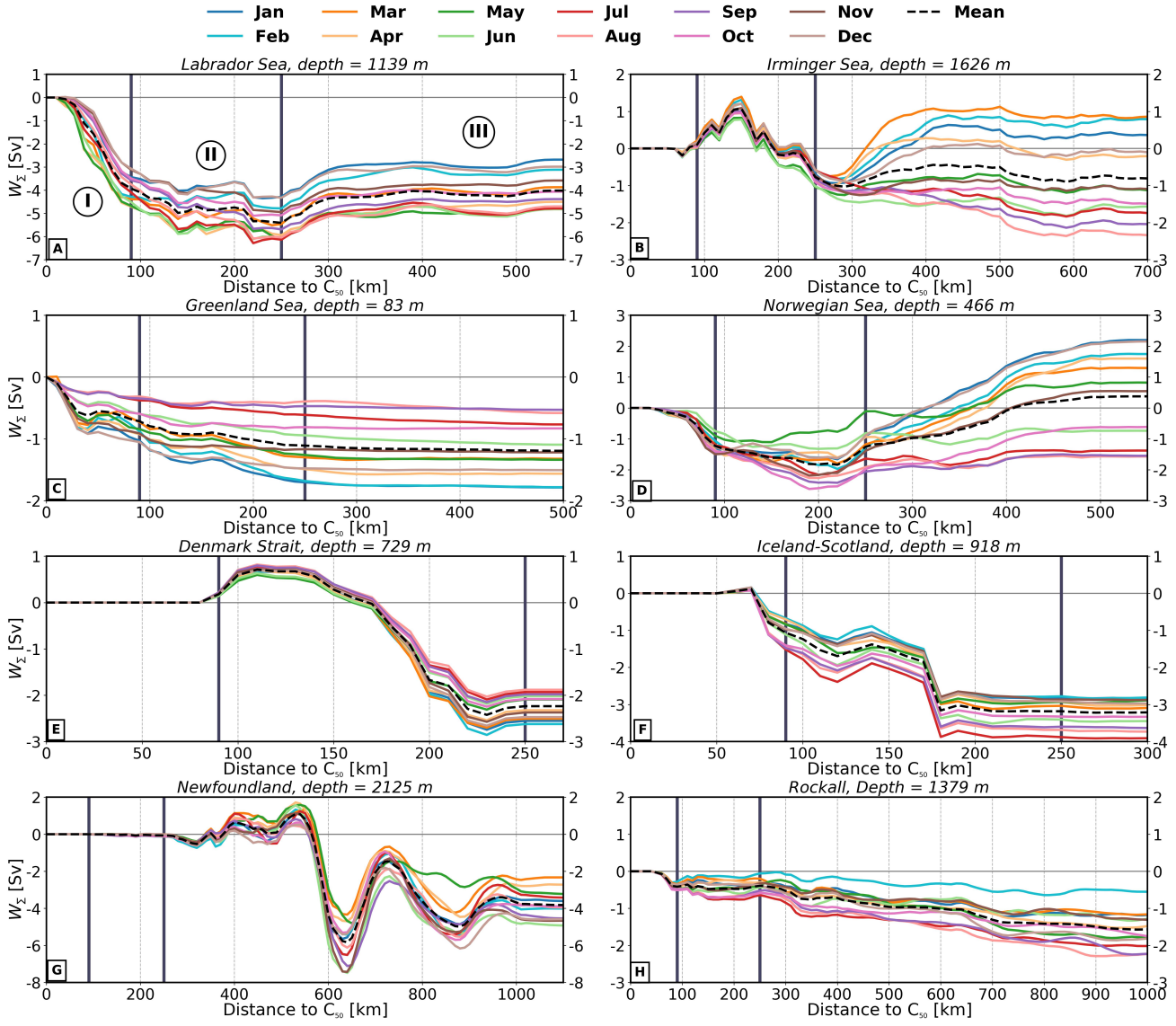

Figure 8. Accumulated net vertical transport (W_Σ) with respect to the distance to the closest ~~land point~~bathymetric contour of 50 m (C_{50}). Distances are ~~based on~~ shown in Fig. 4 (inset map). Annual (dashed black line) and monthly mean (colored lines) curves are depicted for the regions defined in Fig. 6. The accumulated W_Σ has been calculated at the depth of minimum time-mean W_Σ ($z_{\min}$), which differs for each region (see Table 2 and plot title). The bounds separating the sinking regimes (**I-II-III**) proposed in Fig. 4 (~~110~~ 90 km, ~~290~~ 250 km) are indicated with thicker solid vertical lines. Note the differences in the horizontal and vertical scales in the plots.

In Iceland-Scotland the ~~sinking regimes **I** and **III**~~ strongest sinking can be identified for distances to ~~the coast~~ C_{50} smaller than 100 km ~~and between 250 and 500 km respectively — note the two sill steps that appear~~ but relatively far when compared with Labrador and Norwegian Seas. Sinking is larger in summer than in winter. The two sills are clearly identifiable in Fig. ~~9F:~~

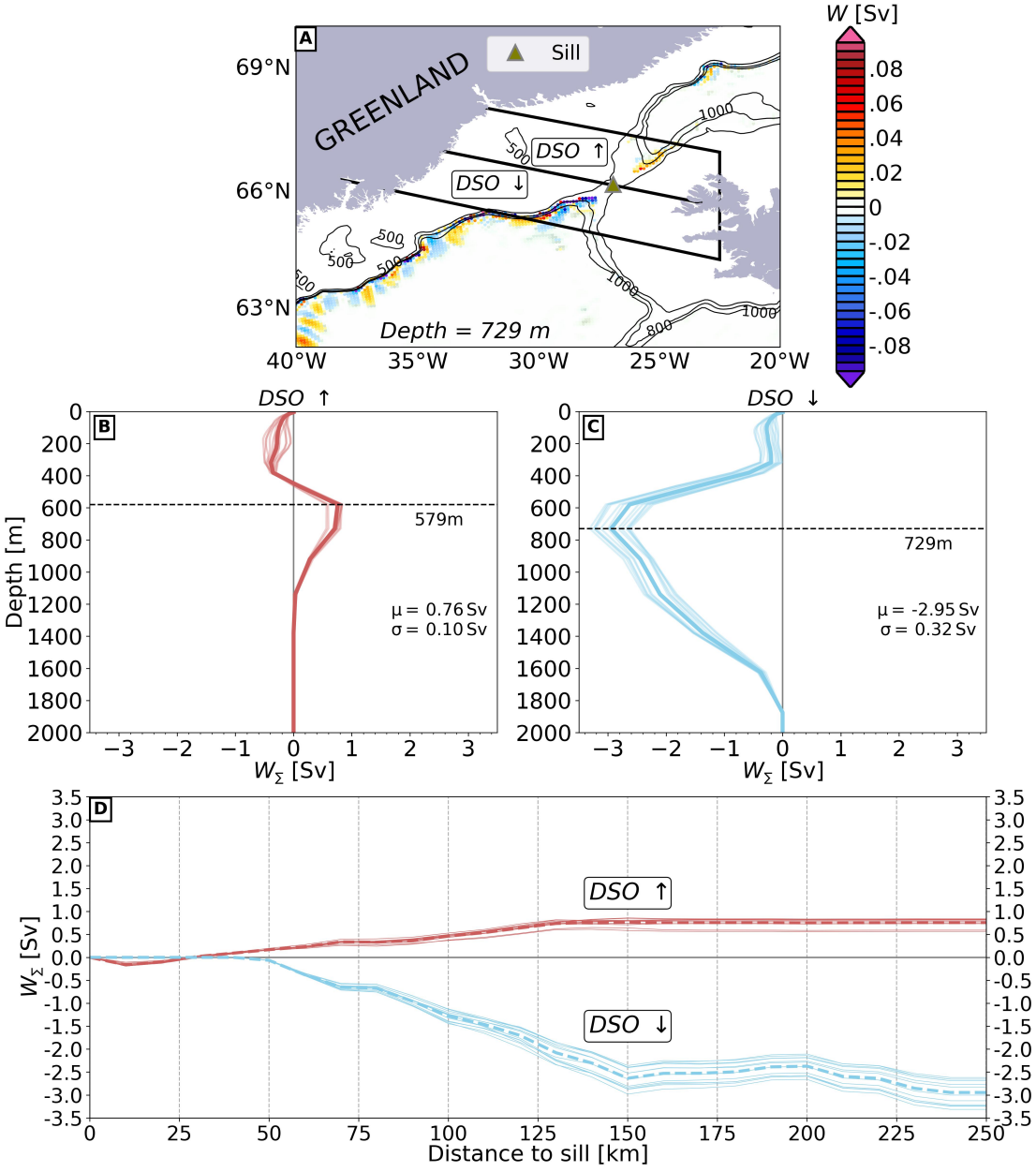

Figure 9. (A) Map of Denmark Strait Overflow region (DSO). The mean vertical transport (W) at 729 m is depicted by shading (color). The triangle illustrates the location of the sill (green triangle) that separates the Denmark Strait in two areas of similar size (DSO ↑ and DSO ↓). Bathymetric contours are indicated by black line. (B-C) Vertical structure of transport (W $in DSO\uparrow$ and DSO ↓ respectively. (D) Annual (dashed line) and monthly (red solid lines) accumulated vertical transport with respect to the sill in DSO ↑ (red) and in DSO ↓ (light blue). Both have been calculated at the corresponding depths of largest upwelling (579 m) and sinking (729 m) for DSO ↑ and DSO ↓ respectively.

~~one near Iceland at ~ 80 km , and the other near~~ 8F: the first near Scotland at ~~~ 200 km—. The distinction between regimes I~~ around 80 km and ~~H is hardly applicable to the Denmark Strait due to the major importance of the overflow waters~~the second near Iceland at about 180 km from C_{50}. So our results ~~suggest that the sinking regimes do~~ indicate that the classification in sinking regimes does not capture some specific features of the overflows. This is not surprising, since they are governed by a different dynamics. Indeed, the location where sinking associated with overflows occurs is not determined by lateral boundaries but rather by the bathymetry, so that it can occur at distances to the ~~coast~~ shelf distinct from the pattern shown by the marginal seas.

4.3 Mid-latitude seas

~~Newfoundland is~~ Finally, we discuss the characteristics of the vertical transport in two regions at mid-latitudes: Newfoundland, located further south ~~,~~ in the vicinity of the Gulf Stream, ~~while Rockall~~and Rockall, which occupies the east Atlantic between 5°W and 25° ~~W~~south of Iceland. Together they yield a time-mean W_Σ contribution of ~~~ -4.8~~ ~ -5.4 Sv at $z_{\min}$ (Fig. 7G-H). Newfoundland is the region with the second largest W_Σ after the Labrador Sea, with a sinking of ~~-3.7 Sv~~ -3.8 Sv. About -0.5 Sv of the sinking contained in Rockall takes place near the south of Iceland. A significant difference between both regions is $z_{\min}$, which is much deeper in Newfoundland (2125 m) than in Rockall (1379 m). Indeed sinking extends deeper in Newfoundland, even reaching depths below 3000 m (Fig. 7G). The minimum (maximum) W_Σ at $z_{\min}$ occurs in summer (winter) for both areas, being in June (March) and August (February) for Newfoundland and Rockall respectively. Although monthly variations reach 4 Sv for Newfoundland and 2 Sv for Rockall (solid curves in Fig. ~~8G-H~~S8G-H), the seasonal cycle is not very pronounced for either of the two regions at $z_{\min}$, although clearer for Rockall. The much larger temporal variability for Newfoundland is reflected in ~~$\sigma = 1.85$~~ $\sigma = 1.86$ Sv against the ~~$\sigma = 0.59$~~ $\sigma = 0.65$ Sv of Rockall, despite the SNR is ~~almost the same~~ rather similar (2 against ~~1.8~~2.4).

Clear differences are seen when we compare the accumulated W_Σ with respect to the distance to ~~the coast~~ C_{50} (Fig. ~~9G-H~~ 8G-H for the two regions). Interestingly, Newfoundland displays large oscillations of positive and negative accumulated W_Σ with wavelengths of about 200 km. This suggests the presence of permanent mesoscale eddies in the ocean interior, which are able to induce those such strong vertical velocities, as shown in Fig. 5. In contrast, Rockall shows on average a quasi-linear decrease of the mean accumulated W_Σ with respect to the distance to ~~the coast~~C_{50} that is more intense in the area within regime I. It also displays seasonal variability that, for example, yields a smaller sinking during late winter and spring months. We conclude that mean features of sinking in Newfoundland and Rockall regions show similar characteristics to those seen for the entire subpolar North Atlantic, as reflected by some boundary sinking in Rockall (regime **I**) and the strong ~~eddy-induced velocities~~ vertical velocities at large, semi-permanent eddies likely detached from the North Atlantic Current in the interior of Newfoundland (regime **III**).

4.4 Further characterization of sinking regimes illustrated by selected regions

In this Section we discuss in more detail the differences in sinking based on three regions: the Labrador and Irminger Seas, and Newfoundland. These regions represent around 2/3 of the total sinking, are relatively far from overflows (although some con-

tribution may be expected in the northern Irminger Sea~~may be expected~~) and present remarkable differences in their dominant sinking regimes covering a wide range of patterns that can be ~~extended to~~ identified in other marginal seas as well. The spatial distribution of time-mean vertical transport (W) for the three regions at the corresponding depth of largest sinking ($z_{\min}$), which differs for each region according to Table 2, is shown in Fig. 10A; the difference between the W calculated during the months of minimum and maximum W_Σ is shown in Fig. 10B (also these months, distinct for each region, are indicated in Table 2). We have added black contours to illustrate the positive/negative variation of the climatological mean EKE between the respective months at $z_{\min}$ (Fig. 10B).

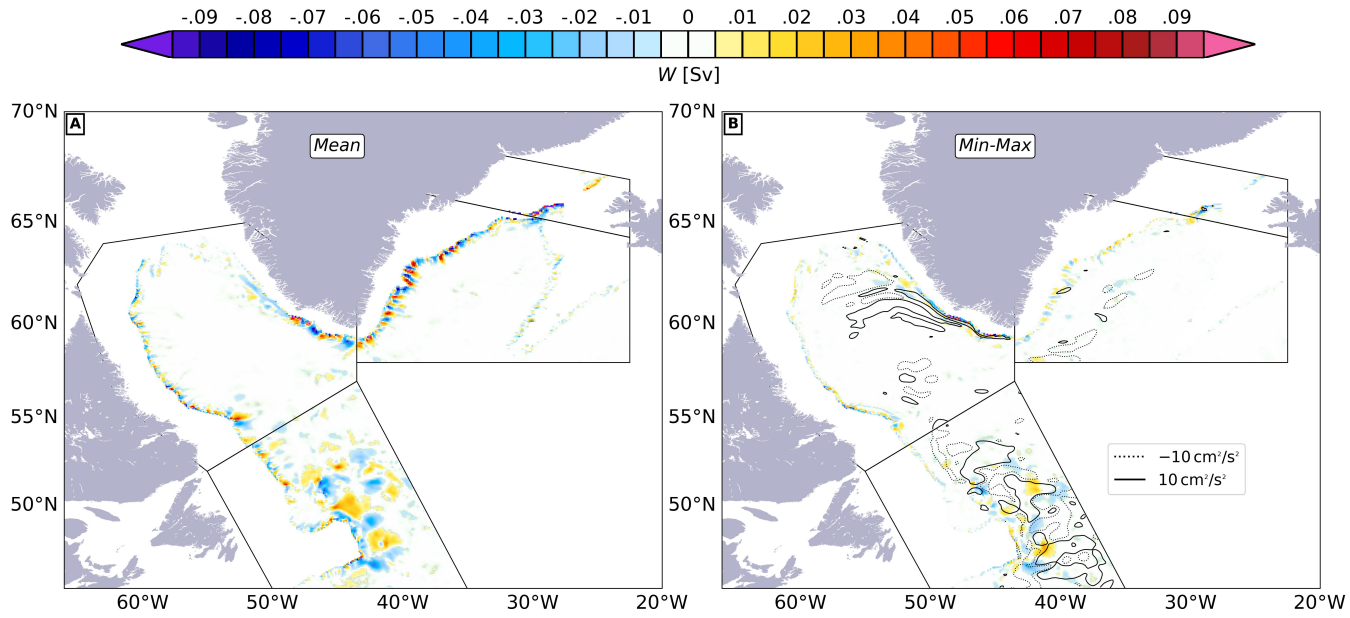

Figure 10. (A) Composite map of mean vertical transport (W) for the western regions of study (defined in Fig. 6) at the corresponding depth of minimum time-mean W_Σ, which differs for each region according to Table 2. (B) Same as (A) but now the mean W (shading) and EKE (blacks contours, see legend) at the month of minimum W_Σ minus the mean W at the month of maximum W_Σ is plotted. These months of minimum and maximum sinking also change for each region according to Table 2. Units of W in Sv and of EKE in $\mathrm{cm}^2 \cdot \mathrm{s}^{-2}$.

The Labrador Sea, which yields the largest contribution to the time-mean W_Σ, is the most representative sea where all the necessary ingredients for boundary sinking are fulfilled: a cyclonic boundary current, strong along-shore and cross-shore density gradients, a steep bathymetric slope ~~,~~ and an active eddy field ~~, and strong along-shore and cross-shore density gradients (Brüggemann and Katsman, 2019)~~(Brüggemann and Katsman, 2019; Georgiou et al., 2019). As a result, the three sinking regimes proposed for the entire subpolar North Atlantic in Fig. 4 were also identified in Fig. 10A for the Labrador Sea. The strong W near the boundary in the Labrador Sea (Fig. 10A) intensifies at the western side of the southern tip of Greenland during late spring, which is associated with a nearby increase of EKE (see the solid black contours over the blue patches in Fig. 10B, and the patches of EKE in Fig. ~~S4C-E~~ S5C-E around the tip). Indeed the Labrador Sea displays an increase in the average horizontal speed of the boundary current at $z_{\min}$ during late winter and spring (Fig. 11A), which may enhance

the horizontal velocity shear. As a result, we can expect an increase in the mean advection of vorticity between the coast and near the peak of the boundary current (at around ~~90 km~~ 70 km off C_{50}, mostly within the region covered by regime **I**, Fig. 11A) and a decrease offshore of the location of the maximum speed (~~mostly~~ with a part within the regime **II**) that may be compensated by the presence of more eddies. The more active role of eddies exchanging waters between the interior and the boundary agrees with the reduced cross-shore potential density gradients found in regions **I** and **II** (green and orange lines in Fig. 11B). The idea that changes in EKE pathways may facilitate to intensify sinking is further discussed by Georgiou et al. (2019) for an idealized convective basin mimicking the Labrador Sea.

In contrast to the Labrador Sea, the change in W in the Irminger Sea between the months of minimum and maximum time-mean W_Σ is significantly smaller (Fig. 10B). This finding, together with the permanent depth of largest sinking ($z_{\min}$) and the up and down distribution of sinking found in Fig. ~~9B~~ 8B, supports the hypothesis that the sinking near the boundary in the Irminger Sea is mostly quasi-stationary and topographically-driven (see a detailed example of this up/down of waters in Fig. S9), which explains the small amount of net sinking found. In Fig. ~~9B~~ 8B it can be observed that there is a large difference (in terms of seasonal variability) between the sinking regimes **I-II** and the regime **III** in the Irminger Sea, which is probably driven by interior eddies. An interesting point to mention is the ~~strong~~ stronger mixing of waters within regions of regimes **I-II** (or equivalently, the reduction of the cross-shore gradient) during the months of late winter and spring (orange and green lines in Fig. 11D). This pattern reflects a different behavior from what we find in the Labrador Sea or Newfoundland (Fig. 11B,F) and is accompanied by an intensification of the boundary current during the same months (orange and green lines in Fig. 11C). This difference is also reflected in the positive vertical transport during winter within the regime **II** (blue and orange lines in Fig. ~~9B~~8B) and reinforces the crucial importance of topographic features in driving the boundary sinking in the Irminger Sea.

Newfoundland yields the second largest contribution to sinking, which is largely produced within the sinking regime **III**. The strong seasonal variations of W in the Newfoundland region below 2000 m are mostly related to EKE interior pathway changes (see black contours in Fig. 10B) impinged by North Atlantic Current fluctuations and meandering. ~~This active contribution of the large interior eddies in inducing these up and down strong vertical velocities~~ The fact that strong vertical velocities appear at the edge of large eddies in the interior, thus contributing to upwelling/sinking has been already shown in Fig. 9G~~(also in Fig. 2A~~, Fig. 10A-B and Fig. ~~5), and is clear from Fig. 10A-B~~ S4, where a train of large eddies near the Flemish Cap is visible~~(also here the strong EKE variations are denoted by the black contours~~). Finally, in the Newfoundland region the peak of the boundary current at its corresponding $z_{\min}$ falls in regime **III** (Fig. 11E); although the ~~largest to the boundary~~ strongest sinking occurs in the interior and below 2000 m, there is some sinking at shallower depths as indicated by its vertical structure in Fig. 7G (Fig. S4). Similar plots showing the overall weaker spatial patterns of sinking for the remainder of the regions can be found in Fig. ~~S7~~ S10 and Fig. ~~S8~~S11.

5 Are regional variations in the net vertical transport connected to AMOC changes?

In Sect. 3 we demonstrated the consistency between the overturning streamfunction (ψ_o) at the southern boundary of our study area at 45°N and the total net vertical transport (W_Σ) in the subpolar Atlantic basin (Fig. 3B). As the amount of accumulated

negative W_Σ appeared to differ between the boundaries and the interior, we have classified the sinking according to three regimes (Fig. 4). Moreover, in Sect. 4 we have evaluated the spatial patterns and the seasonal variability of sinking at the regional level. The fact that nearby areas exhibit striking differences in the amount, the seasonality and the distribution of W_Σ suggests that, to a large extent, it depends on local dynamics and bathymetry. However, it still remains unclear how regional boundary sinking is related to the AMOC strength. For instance, does a decrease/increase in Labrador Sea W_Σ have any quantifiable effect on the AMOC? To address this we have computed the cross-correlation between the reverted time series of the maximum of ψ_o at $45°$N (red lines in Fig. 3B) and the time series of W_Σ (Fig. 8) for each region at the depth of largest sinking ($z_{\min}$, Table 2). We have performed the analysis for two cases: with seasonal variability (Fig. 12B) and without seasonal variability (Fig. 12C). Fig. 12A shows the monthly climatology of sinking at their corresponding $z_{\min}$ so that the months with the largest and smallest sinking for all regions (Table 2) are easily identifiable. Solid lines in Fig. 3B and in Fig. 9 include the seasonal signal whereas in the dashed lines seasonality has been subtracted. A positive correlation at a positive time-lag τ means that stronger (weaker) sinking yields a stronger (weaker) AMOC (ψ_o) at $45°$N τ months later.

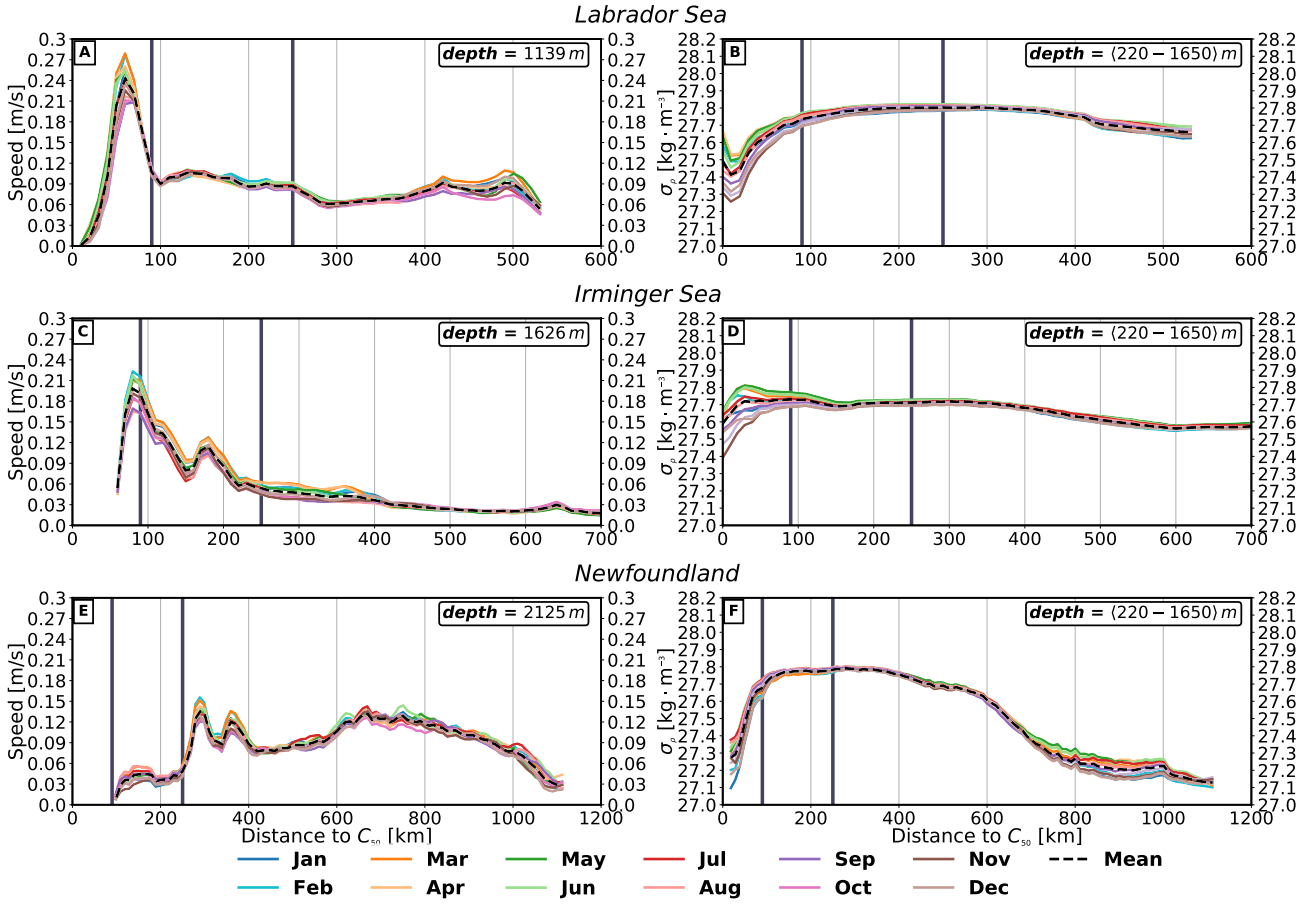

Figure 11. 15-year climatology of the following variables with respect to the distance to the coast (according to the inset map in Fig. 4) for (A)-(B) the Labrador Sea, (C)-(D) the Irminger Sea, and (E)-(F) Newfoundland: (A)-(C)-(E) horizontal speed of current at the depth of largest sinking ($z_{\min}$, Table 2); (B)-(D)-(F) potential density anomalies ($\sigma_\rho = \rho - 1000$ [kg $\cdot$ m^{-3}]) averaged between z-layers 14 and 24 ($\sim 220 - 1650$ m). For all panels the dashed black line depicts the mean, whereas colored lines show the monthly average. The bounds between the sinking regimes proposed in Fig. 4 are indicated with thicker solid vertical lines. Note the differences in horizontal scales of the subpanels.

The high correlation between W_Σ for the entire subpolar North Atlantic (DOMAIN) and ψ_o (> 0.9, mentioned in Sect. 3) appears clearly at zero-lag for both study cases. Also the time-lags found for regions are in agreement with the temporal separation between the corresponding months of minimum W_Σ and the month of maximum ψ_o at 45°N. For instance, the Labrador Sea displays the minimum sinking in June whereas ψ_o has its maximum in August (Fig. 12A). As a consequence, the highest correlation is found for a lag of the AMOC of 1-2 months. The same is found for all other regimes, including the Denmark Strait, which has the minimum W_Σ in February yielding a negative correlation at zero-lag. Fig. 12B shows that for the southern regions (Rockall and Newfoundland) correlations are surprisingly weak. One reason for this is that the signal of negative W_Σ is very noisy for these two regions, with no clear seasonal cycle (Fig. ~~8G-H~~S8G-H), while ψ_o has a clear seasonal

signature. Also for the Greenland Sea correlations are rather weak (< 0.4), presumably due to its small seasonal variability (Fig. ~~8C~~S8C).

To eliminate the influence of seasonality we repeat the analysis on the deseasoned signal. Resulting correlations (Fig. 12C) demonstrate that the only region with a significant correlation between variations of sinking and ψ_o is Newfoundland. This is the region with the largest non-seasonal variations (Fig. ~~8G~~S8G, dashed line) and that shares its boundary with ψ_o at $45°$N. Therefore it is reasonable to think that any change in the North Atlantic Current, either in strength or position, will reflect in sinking in Newfoundland and vice versa (for instance a fluctuation in the train of eddies ~~nearby the Flemish Cap~~in the interior of the Newfoundland region).

The existence of a high correlation does not necessarily ~~implies~~ imply that variations in the sinking waters govern the AMOC as the different regions in this simulation are subject to the same strong large-scale forcing, for instance the seasonal heat fluxes or wind stress variations that affect mid and high North Atlantic latitudes. Thus, the AMOC and the sinking are likely responding synchronously to variations in large-scale forcing. Therefore our results using an Eulerian standpoint do not evidence that a variation (marked increase/decrease) in W_Σ at any of the marginal seas propagates to the lower cell of the AMOC. To investigate this in more detail requires the use of a Lagrangian approach to track the boundary sinking and subsequent spreading of waters, which is beyond the scope of this paper.

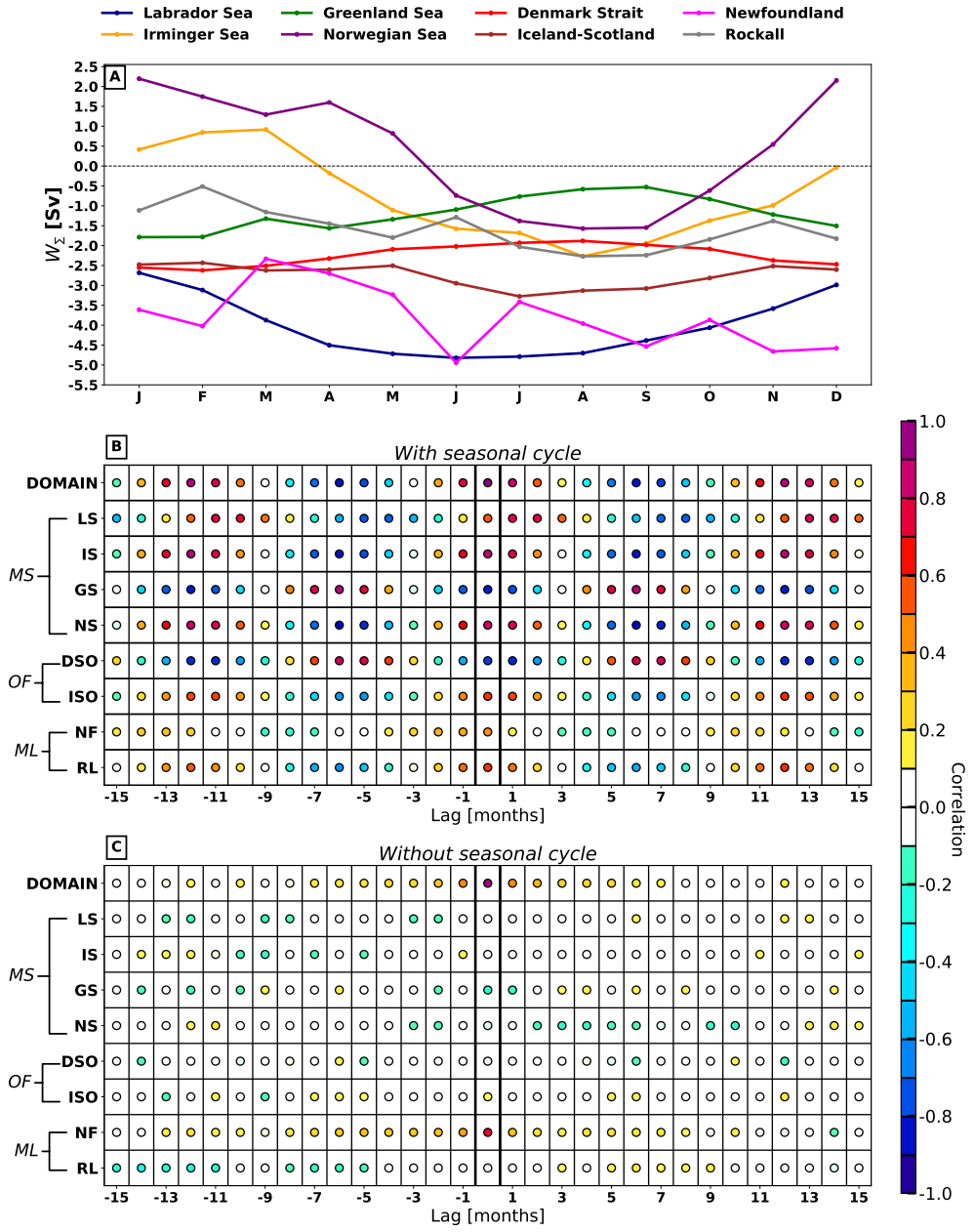

Figure 12. (A) Time series of the monthly climatology of W_Σ for the regions defined in Fig. 6 at the depth of largest mean sinking ($z_{\min}$, which differs between regions according to Table 2). (B) Cross-correlation between the maximum of the reverted overturning streamfunction (ψ_0) at 45°N (red lines in Fig. 3B) and the regional time series of net vertical transport, W_Σ (Fig. 8S8), at the depth of minimum time-mean sinking for a set of time-lags (in months). (C) As (B) but without the seasonal variability. The seasonality has been removed by subtracting the corresponding 15-year monthly mean (i.e. panel (A) for the regional time series). Sinking leads over ψ_0 for positive lags. DOMAIN refers to the whole study area (Fig. 6) and the acronyms are defined as: Labrador Sea (LS), Irminger Sea (IS), Greenland Sea (GS), Norwegian Sea (NS), Denmark Strait overflow (DSO), Iceland-Scotland Ridge overflow (ISO), Newfoundland (NF) and Rockall (RL), marginal seas (MS), overflow regions (OF) and mid-latitude seas (ML).

6 Summary and discussion

Based on a high resolution ocean model simulation forced by a prescribed annual cycle of wind, precipitation and heat fluxes, we have found that the amount of minimum time-mean net vertical transport (W_Σ) for the entire subpolar North Atlantic Ocean is consistent with the transport and vertical structure of the AMOC core at mid latitudes (45°N), with an average of about -14 Sv at a depth of 1139 m. Moreover, the prescribed annual cycle introduces a strong seasonality that favours more sinking of waters at basin scale and a stronger AMOC during summer than in winter, with a similar seasonal variability in both signals (~ 10 Sv). However, this picture becomes much more complex at regional scales, as is illustrated by the different depths at which the largest sinking occurs (ranging from 460 to 2000 m), the distinct spatial distribution and the asynchronous seasonal variations of W_Σ that are found for the different regions in the subpolar North Atlantic.

In accordance with recent studies, our model results confirm that the largest vertical transports occur near the boundaries below the mixed layer depth (Katsman et al., 2018; Brüggemann and Katsman, 2019; Georgiou et al., 2019), in a narrow band that extends between 50 and ~~300~~ 250 km off the ~~coastline~~contour of 50 m depth (C_{50}). When we consider the sinking over the whole subpolar North Atlantic, three dominant sinking regimes are revealed: regime **I** (~~$\sim 0-100$~~ $\sim 0-90$ km) appears where the ~~continental slope is steepest~~topographic dissipation is largest, regime **II** (~~$\sim 100-300$~~ $\sim 90-250$ km) covers the remainder of the continental slope, and regime **III** (distances > ~~300~~ 250 km) occurs in the ocean interior. Our results indicate that around the 90% of the accumulated sinking takes place in the area covered by regions **I** and **II**, while the largest seasonal variability of sinking occurs in region **III**. The near-boundary sinking in regimes **I** and **II** is thought to be governed by the ageostrophic dynamics discussed by e.g. Spall and Pickart (2001) and Straneo (2006), and its amount depends on the interplay of several factors: the existence of a boundary current~~on a pronounced topographic~~ , a steep slope, the presence of eddies, and ~~on~~ the along-shore and cross-shore density gradients (sloping isopycnals)~~near the slope~~. This implies that the budget of W_Σ is potentially sensitive to the intensity and the width of the boundary current, the strength of the eddy field, and the dominant eddy paths (Georgiou et al., 2019).

Distinguishing by regions, we find that most of sinking occurs in the Labrador Sea (~ -4.0 Sv), Newfoundland (~~~ -3.7~~ ~ -3.8 Sv) and the overflow regions (Denmark Strait and Iceland-Scotland Ridge with ~~~ -2.2 Sv each~~~ -5 Sv altogether). The Irminger and Norwegian Seas show a strong seasonally-dependent behaviour, with sinking during part of the year and upwelling the rest of the year and hence little net sinking. We identified the three sinking regimes in almost all regions except in the overflow regions, which are governed by a different dynamics, and in the Irminger Sea. The Irminger Sea shows a distinct sinking dynamics near the boundary due to the existence of bathymetry-forced flows and probably by some overflow waters coming from the Denmark Strait. Moreover, in each region the distance from the coast that marks the boundary between the sinking regimes is seen to shift due to the local dynamics and bathymetric features (e.g. different steepness or shelf width) of each region.

The dominance of the seasonal forcing in the sinking response (probably induced by the repeated forcing conditions) ~~limits us to find~~ prevents us from finding a connection between the regional variations of sinking and the lower cell of the AMOC at mid latitudes, though previous research has suggested a complex interaction between the surface atmospheric forcing, the

boundary current and interior waters for which eddies play a crucial role (Georgiou et al., 2019). To gain insight into this connection would require an analysis of the near-boundary sinking and the AMOC in a model simulation with varying surface forcing. In addition, we have studied the Eulerian net vertical transport without referring to the water-mass properties while the subpolar North Atlantic is characterized by a strong densification of waters during late winter and spring. The latter would require an assessment of sinking in density space, which is outside the main scope of this study, which focuses only on the vertical structure, seasonality and spatial distribution of sinking. Also we note that monthly fields neither allow to quantify accurately which waters are sinking, nor the amount of isopycnal and diapycnal mixing, since isopycnals ~~significantly fluctuate~~ fluctuate significantly at shorter time scales. In this regard, our next step aims to address the above points by tracking the waters sinking near the boundary using a simulation with higher temporal resolution. With this analysis, we expect to identify the characteristics of the near-boundary sinking water masses, and to assess if any of their preferred pathways take them to the lower limb of the AMOC.

Author contributions. JMS and CAK designed the paper, HAD provided the model data, JMS performed the data analysis, JMS and CAK interpreted the results and wrote the paper. All authors have read and approved the submitted version of the manuscript.

Competing interests. The authors declare that no competing interests are present.

Acknowledgements. J.-M. Sayol and C. A. Katsman thank the financial support by the Netherlands Scientific Research foundation (NWO) through the VIDI grant number 864.13.011 awarded to C.A. Katsman. Help in data processing from M. Kliphuis and comments from N. Brüggemann, S. Georgiou, S. Ypma and C. van der Boog on the analysis and the manuscript are greatly appreciated.

References

Adcroft, A., Hill, C., and Marshall, J.: Representation of Topography by Shaved Cells in a Height Coordinate Ocean Model, Monthly Weather Review, 125, 2293–2315, https://doi.org/10.1175/1520-0493(1997)125<2293:ROTBSC>2.0.CO;2, 1997.

Azetsu-Scott, K., Petrie, B., Yeats, P., and Lee, C.: Composition and fluxes of freshwater through Davis Strait using multiple chemical tracers, Journal of Geophysical Research: Oceans, 117, https://doi.org/10.1029/2012JC008172, 2012.

Bower, A. S. and Hunt, H. D.: Lagrangian Observations of the Deep Western Boundary Current in the North Atlantic Ocean., Journal of Physical Oceanography, 30, 764–783, https://doi.org/10.1175/1520-0485(2000)030<0764:LOOTDW>2.0.CO;2, 2000.

Bower, A. S., Lozier, M. S., Gary, S. F., and Böning, C. W.: Interior pathways of the North Atlantic meridional overturning circulation, Nature, 459, 243–247, https://doi.org/10.1038/nature07979, 2009.

Brambilla, E. and Talley, L. D.: Surface drifter exchange between the North Atlantic subtropical and subpolar gyres, Journal of Geophysical Research: Oceans, 111, https://doi.org/10.1029/2005JC003146, 2006.

Broecker, W. S.: The Biggest Chill: When Ocean Currents Shifted, Europe Suddenly Got Cold; Could it Happen Again?, Natural History, 96, 9, 1987.

Broecker, W. S.: The Great Ocean Conveyor, Oceanography, 4, 79–89, https://doi.org/10.5670/oceanog.1991.07, 1991.

Brüggemann, N. and Katsman, C. A.: Dynamics of downwelling in an eddying marginal sea: contrasting the Eulerian and the isopycnal perspective, Submitted to Journal of Physical Oceanography, 2019.

Brüggemann, N., Katsman, C. A., and Dijkstra, H. A.: On the vorticity dynamics of the downwelling branch of the AMOC, CLIVAR Exchanges Special Issue: CLIVAR Open Science Conference Award Winners, 71, 10–12, 2017.

Brunnabend, S.-E. and Dijkstra, H. A.: Asymmetric response of the Atlantic Meridional Ocean Circulation to freshwater anomalies in a strongly-eddying global ocean model, Tellus A: Dynamic Meteorology and Oceanography, 69, 1299 283, https://doi.org/10.1080/16000870.2017.1299283, 2017.

Buckley, M. W. and Marshall, J.: Observations, inferences, and mechanisms of the Atlantic Meridional Overturning Circulation: A review, Reviews of Geophysics, 54, 5–63, https://doi.org/10.1002/2015RG000493, 2016.

Cenedese, C.: Downwelling in Basins Subject to Buoyancy Loss, Journal of Physical Oceanography, 42, 1817–1833, https://doi.org/10.1175/JPO-D-11-0114.1, 2012.

Cunningham, S. A., Kanzow, T., Rayner, D., Baringer, M. O., Johns, W. E., Marotzke, J., Longworth, H. R., Grant, E. M., Hirschi, J. J.-M., Beal, L. M., Meinen, C. S., and Bryden, H. L.: Temporal Variability of the Atlantic Meridional Overturning Circulation at 26.5°N, Science, 317, 935–938, https://doi.org/10.1126/science.1141304, 2007.

de Boyer Montégut, C., Madec, G., Fischer, A. S., Lazar, A., and Iudicone, D.: Mixed layer depth over the global ocean: An examination of profile data and a profile-based climatology, Journal of Geophysical Research: Oceans, 109, https://doi.org/10.1029/2004JC002378, 2004.

Frajka-Williams, E., Eriksen, C. C., Rhines, P. B., and Harcourt, R. R.: Determining Vertical Water Velocities from Seaglider, Journal of Atmospheric and Oceanic Technology, 28, 1641–1656, https://doi.org/10.1175/2011JTECHO830.1, 2011.

Georgiou, S., van der Boog, C. G., Brüggemann, N., Ypma, S. L., Pietrzak, J. D., and Katsman, C. A.: On the interplay between downwelling, deep convection and mesoscale eddies in the Labrador Sea, Ocean Modelling, 135, 56 – 70, https://doi.org/https://doi.org/10.1016/j.ocemod.2019.02.004, 2019.

Holliday, N. P., Bacon, S., Cunningham, S. A., Gary, S. F., Karstensen, J., King, B. A., Li, F., and Mcdonagh, E. L.: Subpolar North Atlantic Overturning and Gyre-Scale Circulation in the Summers of 2014 and 2016, Journal of Geophysical Research: Oceans, 0, https://doi.org/10.1029/2018JC013841, 2018.

Holte, J. and Straneo, F.: Seasonal Overturning of the Labrador Sea as Observed by Argo Floats, Journal of Physical Oceanography, 47, 2531–2543, https://doi.org/10.1175/JPO-D-17-0051.1, 2017.

Holte, J., Talley, L. D., Gilson, J., and Roemmich, D.: An Argo mixed layer climatology and database, Geophysical Research Letters, 44, 5618–5626, https://doi.org/10.1002/2017GL073426, 2017.

Håvik, L., Våge, K., Pickart, R. S., Harden, B., Appen, W., Jónsson, S., and Østerhus, S.: Structure and Variability of the Shelfbreak East Greenland Current North of Denmark Strait, Journal of Physical Oceanography, 47, 2631–2646, https://doi.org/10.1175/JPO-D-17-0062.1, 2017.

Jochumsen, K., Quadfasel, D., Valdimarsson, H., and Jónsson, S.: Variability of the Denmark Strait overflow: Moored time series from 1996-2011, Journal of Geophysical Research: Oceans, 117, https://doi.org/10.1029/2012JC008244, 2012.

Jochumsen, K., Moritz, M., Nunes, N., Quadfasel, D., Larsen, K. M. H., Hansen, B., Valdimarsson, H., and Jonsson, S.: Revised transport estimates of the Denmark Strait overflow, Journal of Geophysical Research: Oceans, 122, 3434–3450, https://doi.org/10.1002/2017JC012803, 2017.

Kanzow, T., Cunningham, S. A., Johns, W. E., Hirschi, J. J.-M., Marotzke, J., Baringer, M. O., Meinen, C. S., Chidichimo, M. P., Atkinson, C., Beal, L. M., Bryden, H. L., and Collins, J.: Seasonal Variability of the Atlantic Meridional Overturning Circulation at 26.5°N, Journal of Climate, 23, 5678–5698, https://doi.org/10.1175/2010JCLI3389.1, 2010.

Katsman, C., Drijfhout, S. S., Dijkstra, H. A., and Spall, M. A.: Sinking of Dense North Atlantic Waters in a Global Ocean Model: Location and Controls, Journal of Geophysical Research: Oceans, 123, 3563–3576, https://doi.org/10.1029/2017JC013329, 2018.

Köhl, A., Käse, R. H., Stammer, D., and Serra, N.: Causes of Changes in the Denmark Strait Overflow, Journal of Physical Oceanography, 37, 1678–1696, https://doi.org/10.1175/JPO3080.1, 2007.

Kornei, K.: Ocean array alters view of Atlantic conveyor, Science, 359, 857–857, https://doi.org/10.1126/science.359.6378.857, 2018.

Large, W. G. and Yeager, S.: Diurnal to decadal global forcing for ocean and sea-ice models: The data sets and flux climatologies, Tech. rep., National Center for Atmospheric Research, Boulder, CO, USA, 2004.

Lozier, M. S.: Deconstructing the Conveyor Belt, Science, 328, 1507–1511, https://doi.org/10.1126/science.1189250, 2010.

Lozier, M. S.: Overturning in the North Atlantic, Annual Review of Marine Science, 4, 291–315, https://doi.org/10.1146/annurev-marine-120710-100740, 2012.

Lozier, M. S., Bacon, S., Bower, A. S., Cunningham, S. A., Femke de Jong, M., de Steur, L., de Young, B., Fischer, J., Gary, S. F., Greenan, B. J. W., Heimbach, P., Holliday, N. P., Houpert, L., Inall, M. E., Johns, W. E., Johnson, H. L., Karstensen, J., Li, F., Lin, X., Mackay, N., Marshall, D. P., Mercier, H., Myers, P. G., Pickart, R. S., Pillar, H. R., Straneo, F., Thierry, V., Weller, R. A., Williams, R. G., Wilson, C., Yang, J., Zhao, J., and Zika, J. D.: Overturning in the Subpolar North Atlantic Program: A New International Ocean Observing System, Bulletin of the American Meteorological Society, 98, 737–752, https://doi.org/10.1175/BAMS-D-16-0057.1, 2017.

Lozier, M. S., Li, F., Bacon, S., Bahr, F., Bower, A. S., Cunningham, S. A., de Jong, M. F., de Steur, L., deYoung, B., Fischer, J., Gary, S. F., Greenan, B. J. W., Holliday, N. P., Houk, A., Houpert, L., Inall, M. E., Johns, W. E., Johnson, H. L., Johnson, C., Karstensen, J., Koman, G., Le Bras, I. A., Lin, X., Mackay, N., Marshall, D. P., Mercier, H., Oltmanns, M., Pickart, R. S., Ramsey, A. L., Rayner, D., Straneo, F., Thierry, V., Torres, D. J., Williams, R. G., Wilson, C., Yang, J., Yashayaev, I., and Zhao, J.: A sea change in our view of overturning in the subpolar North Atlantic, Science, 363, 516–521, https://doi.org/10.1126/science.aau6592, 2019.

Maltrud, M. E., Bryan, F., Hecht, M., Hunke, E., Ivanova, D., McClean, J., and Peacock, S.: Global ocean modelling in the eddying regime using POP, CLIVAR Exchanges, 44, 5–8, 2008.

Maltrud, M. E., Bryan, F., and Peacock, S.: Boundary impulse response functions in a century-long eddying global ocean simulation, Environmental Fluid Mechanics, 10, 275–295, https://doi.org/10.1007/s10652-009-9154-3, 2010.

Marshall, J. and Schott, F.: Open-ocean convection: Observations, theory, and models, Reviews of Geophysics, 37, 1–64, https://doi.org/10.1029/98RG02739, 1999.

Pedlosky, J. and Spall, M. A.: Boundary Intensification of Vertical Velocity in a β-Plane Basin, Journal of Physical Oceanography, 35, 2487–2500, https://doi.org/10.1175/JPO2832.1, 2005.

Pickart, R. S. and Spall, M. A.: Impact of Labrador Sea Convection on the North Atlantic Meridional Overturning Circulation, Journal of Physical Oceanography, 37, 2207–2227, https://doi.org/10.1175/JPO3178.1, 2007.

Rudels, B., Björk, G., Nilsson, J., Winsor, P., Lake, I., and Nohr, N.: The interaction between waters from the Arctic Ocean and the Nordic Seas north of Fram Strait and along the East Greenland Current: results from the Arctic Ocean-02 Oden expedition, Journal of Marine Systems, 55, 1 – 30, https://doi.org/10.1016/j.jmarsys.2004.06.008, 2005.

Rypina, I. I., Pratt, L. J., and Lozier, M. S.: Near-Surface Transport Pathways in the North Atlantic Ocean: Looking for Throughput from the Subtropical to the Subpolar Gyre, Journal of Physical Oceanography, 41, 911–925, https://doi.org/10.1175/2011JPO4498.1, 2011.

Send, U. and Marshall, J.: Integral Effects of Deep Convection, Journal of Physical Oceanography, 25, 855–872, https://doi.org/10.1175/1520-0485(1995)025<0855:IEODC>2.0.CO;2, 1995.

Shapiro, G. I. and Hill, A.: Dynamics of Dense Water Cascades at the Shelf Edge, Journal of Physical Oceanography, 27, 2381–2394, https://doi.org/10.1175/1520-0485(1997)027<2381:DODWCA>2.0.CO;2, 1997.

Sinha, B., Smeed, D. A., McCarthy, G., Moat, B. I., Josey, S., Hirschi, J. J.-M., Frajka-Williams, E., Blaker, A. T., Rayner, D., and Madec, G.: The accuracy of estimates of the overturning circulation from basin-wide mooring arrays, Progress in Oceanography, 160, 101–123, https://doi.org/10.1016/j.pocean.2017.12.001, 2018.

Smeed, D. A., McCarthy, G. D., Cunningham, S. A., Frajka-Williams, E., Rayner, D., Johns, W. E., Meinen, C. S., Baringer, M. O., Moat, B. I., Duchez, A., and Bryden, H. L.: Observed decline of the Atlantic meridional overturning circulation 2004-2012, Ocean Science, 10, 29–38, https://doi.org/10.5194/os-10-29-2014, 2014.

Smeed, D. A., Josey, S. A., Beaulieu, C., Johns, W. E., Moat, B. I., Frajka-Williams, E., Rayner, D., Meinen, C. S., Baringer, M. O., Bryden, H. L., and McCarthy, G. D.: The North Atlantic Ocean Is in a State of Reduced Overturning, Geophysical Research Letters, 45, 1527–1533, https://doi.org/10.1002/2017GL076350, 2018.

Smith, R., Jones, P., Briegleb, B., Bryan, F., Danabasoglu, G., Dennis, J., Dukowic, z, J., Eden, C., Fox-Kemper, B., Gent, P., Hecht, M., Jayne, S., Jochum, M., Large, W., Lindsay, K., Maltrud, M., Norton, N., Peacock, S., Vertenstein, M., and Yeager, S.: The Parallel Ocean Program (POP) Reference Manual: Ocean Component of the Community Climate System Model (CCSM) and Community Earth System Model (CESM), Tech. rep., Los Alamos National Laboratory, National Center for Atmospheric Research, IFM-GEOMAR, Univ. Kiel, University of Colorado-Boulder, Woods Hole Oceanographic Institution, 2010.

Spall, M. A.: Boundary Currents and Watermass Transformation in Marginal Seas, Journal of Physical Oceanography, 34, 1197–1213, https://doi.org/10.1175/1520-0485(2004)034<1197:BCAWTI>2.0.CO;2, 2004.

Spall, M. A.: Buoyancy-Forced Downwelling in Boundary Currents, Journal of Physical Oceanography, 38, 2704–2721, https://doi.org/10.1175/2008JPO3993.1, 2008.